arXiv:1209.0506v1 [cond-mat.mes-hall] 4 Sep 2012

Thermoelectric properties of a chain of coupled quantum dots embedded in a nanowire

David M.-T. Kuo[1,†] and Yia-Chung Chang[2,*]
[1]*Department of Electrical Engineering, and department of physics,*
National Central University, Chungli, 320 Taiwan and
[2]*Research Center for Applied Sciences, Academic Sinica, Taipei, 115 Taiwan*
(Dated: September 5, 2012)

The thermoelectric properties of a chain of coupled quantum dots (CCQD) embedded in a nanowire are theoretically investigated in the Coulomb blockade regime. An extended Hubbard model is employed to simulate the CCQD nanowire system. The charge and heat currents are calculated in the framework of Keldysh Green's function technique. We obtained a closed-form Landauer expression for the transmission coefficient of the CCQD system. The electrical conductance (G_e), Seebeck coefficient (S), thermal conductance, and figure of merit (ZT) are numerically calculated and analyzed in the linear response regime. When thermal conductance is dominated by phonon carriers, the optimization of ZT is determined by the power factor ($pF = S^2G_e$). We find that off-resonant tunneling processes, asymmetrical interdot electron Coulomb interactions, weak interdot hopping strengths and asymmetrical tunneling rates between QDs and electrodes are not favored in the optimization of ZT as a result they suppress the power factor of junction system.

I. INTRODUCTION

Recently, considerable studies have been devoted to seeking efficient thermoelectric materials with the figure of merit (ZT) larger than 3 because there exist potential applications of solid state thermal devices such as coolers and power generators.[1−7] The optimization of ($ZT = S^2G_eT/\kappa$) depends on the thermoelectric response functions; electrical conductance (G_e), Seebeck coefficient (S), and thermal conductance (κ). T is the equilibrium temperature. These thermoelectrical response functions are related to one another. Mechanisms leading to the enhancement of power factor ($pF = S^2G_e$) would also enhance the thermal conductance. Consequently, it is difficult to find ZT above 1 in conventional bulk materials.[1] Nanotechnology development provides a possible means to achieve highly efficient thermoelectric materials. Recently, it has been demonstrated that ZT's of nanostructure composites can reach impressive values (larger than one).[8] In particular, quantum dot superlattice (QDSL) nanowires exhibit an interesting thermoelectric property in that the power factor and thermal conductance become unrelated.[8] Based on this property, one can increase the power factor and decrease the thermal conductance simultaneously to optimize ZT. A ZT value close to 2 in PbSe/PbTe QDSL system was reported.[6]

The reduction of thermal conductance of QDSL was attributed to the increase of phonon scattering rates, resulting from phonon scattering from the nanowire surface states and QD interface states.[1,2] Nevertheless, the relationship between the thermoelectric response functions and QD quantum confinement effect including intradot and interdot Coulomb interactions, electron interdot hopping, and QD size fluctuation remains unclear even though thermoelectric properties of QDSL have been theoretically studied by solving the Boltzmann equation.[9] In ref.[9] authors considered infinite long nanowire and ignored electron Coulomb interactions. In the present study, we investigate the thermoelectric properties of finite number of coupled quantum dots (CQDs) embedded in a nanowire and connected to metallic electrodes, which allow carrier injection into the CQDs. Thermoelectric properties of a single QD and double QDs embedded in a matrix connected to electrodes were previously studied by several efforts.[10−13] However, in realistic QD junctions for thermoelectric application, one needs to consider a large number of serially coupled QDs, otherwise it is not easy to keep the large temperature difference cross junction, which is crucial in the implementation of high efficiency thermoelectric devices.[2]

Here we consider nanoscale semiconductor QDs, in which the energy level separations are much larger than their on-site Coulomb interactions and thermal energies. Thus, only one energy level for each quantum dot needs to be considered. An N-level Anderson model is employed to simulate the system as shown Fig. 1. Because we take into account a thick insulator matrix between two metallic leads (for instance SiO_2 or SiN), direct tunneling currents between two electrodes are prohibited. In general, germanium or silicon QDs can be well growth in SiO_2 (SiN) matrix. The system illustrated in Fig. 1 may find promising applications as thermoelectric devices. When N is infinite, it can be regarded as model system to clarify fundamental physics of one-dimensional strongly-correlated systems, which is one of the most challenging problems in condensate matter physics.[14] For finite number of QDs, the transport properties of such QD molecular is complicate due to nonneglecting electron Coulomb interactions. As a consequence, it is very tedious to do the optimization of ZT. Our analytical form of charge and heat formula provides an efficiency means to deal such difficulties. The derived transport formula still valid in the nonequilibrium regime. In this study, we find that the optimization of ZT value favors the following conditions:(1) QDs with low energy level fluctuations, (2) QD energy levels lie above the Fermi level of electrodes, (3) $\Gamma < t_c \ll U_0$, where t_c, U_0, and Γ are electron interdot hopping strength, on-site electron

Coulomb interaction, and tunneling rate, respectively, and (4) $\Gamma_L = \Gamma_R$ with $\Gamma_L + \Gamma_R$ kept constant, where $\Gamma_L(\Gamma_R)$ is the left (right) tunneling rate.

II. FORMALISM

The Hamiltonian of N coupled QDs connected to metallic electrodes can be described by the combination of extended Hubbard model and Anderson model $H = H_0 + H_{QD}$:

$$\begin{aligned} H_0 &= \sum_{k,\sigma} \epsilon_k a^\dagger_{k,\sigma} a_{k,\sigma} + \sum_{k,\sigma} \epsilon_k b^\dagger_{k,\sigma} b_{k,\sigma} \quad (1) \\ &+ \sum_{k,\sigma} V_{k,1} d^\dagger_{1,\sigma} a_{k,\sigma} + \sum_{k,\sigma} V_{k,N} d^\dagger_{N,\sigma} b_{k,\sigma} + c.c \end{aligned}$$

where the first two terms describe the free electron gas of left and right metallic electrodes. $a^\dagger_{k,\sigma}$ ($b^\dagger_{k,\sigma}$) creates an electron of momentum k and spin σ with energy ϵ_k in the left (right) metallic electrode. $V_{k,\ell}$ ($\ell = 1, N$) describes the coupling between the metallic electrodes and the first (N-th) QD. $d^\dagger_{\ell,\sigma}$ ($d_{\ell,\sigma}$) creates (destroys) an electron in the ℓ-th dot.

$$\begin{aligned} H_{QD} &= \sum_{\ell,\sigma} E_\ell n_{\ell,\sigma} + \sum_{\ell} U_\ell n_{\ell,\sigma} n_{\ell,\bar\sigma} \quad (2) \\ &+ \frac{1}{2} \sum_{\ell,j,\sigma,\sigma'} U_{\ell,j} n_{\ell,\sigma} n_{j,\sigma'} + \sum_{\ell,j,\sigma} t_{\ell,j} d^\dagger_{\ell,\sigma} d_{j,\sigma}, \end{aligned}$$

where E_ℓ is spin-independent QD energy level, and $n_{\ell,\sigma} = d^\dagger_{\ell,\sigma} d_{\ell,\sigma}$. Notations U_ℓ and $U_{\ell,j}$ describe the intradot and interdot Coulomb interactions, respectively. $t_{\ell,j}$ describes the electron interdot hopping. Note that the nearest neighbor interdot hopping and interdot Coulomb interaction are taken into account in Eq. (2).

Using the Keldysh-Green's function technique,[15] the charge current leaving the left and right electrodes in the steady state can be expressed by

$$J_L = \frac{-e}{h} \int d\epsilon \Gamma_L [2 f_L(\epsilon) Im G^r_{1,\sigma}(\epsilon) - i G^<_{1,\sigma}(\epsilon)] \quad (3)$$

and

$$J_R = \frac{-e}{h} \int d\epsilon \Gamma_R [2 f_R(\epsilon) Im G^r_{N,\sigma}(\epsilon) - i G^<_{N,\sigma}(\epsilon)], \quad (4)$$

where $\Gamma_L = \Gamma_1$ and $\Gamma_R = \Gamma_N$ denote, respectively, the tunneling rates of the left electrode to the first QD and the right electrode to the Nth QD, which are assumed to be energy and bias independent for simplicity. $f_{L(R)}(\epsilon) = 1/[e^{(\epsilon - \mu_{L(R)})/k_B T_{L(R)}} + 1]$ denotes the Fermi distribution function for the left (right) electrode. The chemical potential difference is given by $\mu_L - \mu_R = e\Delta V$. $T_{L(R)}$ denotes the equilibrium temperature of the left (right) electrode. e and h denote the electron charge and Planck's constant, respectively. Obviously, tunneling currents are determined by the on-site retarded Green's function ($G^r_{1(N),\sigma}(\epsilon)$) and lesser Green's function ($G^<_{1(N),\sigma}(\epsilon)$). It is not trivial to solve N coupled QDs with electron Coulomb interactions (U_ℓ and $U_{\ell,j}$) and electron interdot hopping ($t_{\ell,j} = t_c$). Conventional Hartree-Fork mean field theory can not resolve the detailed quantum pathes. Our previous approach beyond the mean-field approximation can obtain all Green functions in the closed form solutions for N=2 in the limit of $t_c/U \ll 1$.[12,13] Based on the same approach, we have demonstrated that the charge and heat currents of CCQDs can be expressed as[13]

$$\begin{aligned} J &= \frac{2e}{h} \int d\epsilon \mathcal{T}(\epsilon) [f_L(\epsilon) - f_R(\epsilon)], \quad (5) \\ Q &= \frac{2}{h} \int d\epsilon \mathcal{T}(\epsilon)(\epsilon - E_F - e\Delta V)[f_L(\epsilon) - f_R(\epsilon)], \quad (6) \end{aligned}$$

where $\mathcal{T}(\epsilon) \equiv (\mathcal{T}_{1,N}(\epsilon) + \mathcal{T}_{N,1}(\epsilon))/2$ is the transmission coefficient. $\mathcal{T}_{\ell,j}(\epsilon)$ denotes the transmission function, which can be expressed in terms of the on-site retarded Green's functions, even though $\mathcal{T}_{\ell,j}(\epsilon)$ should be calculated by the on-site retarded and lesser Green's functions. The transmission function in the weak interdot hopping limit ($t_{ij} \ll U$) has the following form,

$$\mathcal{T}_{1,N}(\epsilon) = -2 \sum_{m=1}^{2\times 4^{N-1}} \frac{\Gamma_1(\epsilon)\Gamma^m_{1,N}(\epsilon)}{\Gamma_1(\epsilon) + \Gamma^m_{1,N}(\epsilon)} \mathrm{Im} G^r_{1,m}(\epsilon), \quad (7)$$

where Im means taking the imaginary part of the function that follows, and

$$G^r_{1,m}(\epsilon) = p_{1,m}/(\mu_1 - \Pi_{1,m} - \Sigma^m_{1,N}), \quad (8)$$

where $\mu_1 = \epsilon - E_1 + i\Gamma_1/2$, $\Pi_{1,m}$ denotes the sum of Coulomb energies arising from other electron present in the first QD and its neighborhood, and $\Gamma^m_{1,N}(\epsilon) = -2Im\Sigma^m_{1,N}(\epsilon)$, where $\Sigma^m_{1,N}$ denotes the self energy resulting from electron hopping from QD 1 to QD N through channel m. For electron with spin σ tunneling from the left electrode into level 1 of N serially coupled QD and exit to the right electrode, we have $2 \times 4^{N-1}$ quantum pathes (or channels), since level 1 can be either empty or singly occupied (with spin $-\sigma$) and all other levels can be empty, singly occupied (with spin up or down), and doubly occupied. For the $N = 2$ case, the explicit expressions of probability weights and self energies have been worked out in our previous paper.[13] Here, we generalize the expressions to a CCQD system with arbitrary number of QDs. We found that for the N-QD system, the probability factors $p_{1,m}$ are determined by the following relation

$$(\bar a_1 + \bar b_{1\bar\sigma}) \prod_{\ell=2}^{N} (a_\ell + b_{\ell\sigma} + b_{\ell\bar\sigma} + c_\ell) = \sum_{m=1}^{2\times 4^{N-1}} p_{1,m}, \quad (9)$$

where $\bar{a}_\ell = 1-N_{\ell,\bar\sigma}$, $\bar{b}_{\ell,\bar\sigma} = N_{\ell,\bar\sigma}$, $a_\ell = 1-N_{\ell,\bar\sigma}-N_{\ell,\sigma}+c_\ell$, $b_{\ell,\bar\sigma} = N_{\ell,\bar\sigma} - c_\ell$, $b_{\ell,\sigma} = N_{\ell,\sigma} - c_\ell$. a_ℓ, $b_{\ell,\bar\sigma}$, $b_{\ell,\sigma}$, and c_ℓ describe the probability factor for the ℓ-th QD with no electron, one electron of spin $\bar\sigma$, one electron of spin σ, and two electrons, respectively. $N_{\ell,\sigma}$, $N_{\ell,\bar\sigma}$, and $c_\ell = \langle n_{\ell,\bar\sigma} n_{\ell,\bar\sigma} \rangle$ denote the thermally averaged one-particle occupation numbers for spin σ and $\bar\sigma$ and two-particle correlation functions. We note that the sum of Eq. (9) equals one, which indicates probability conservation. $\Sigma^m_{1,N}$ is given by a continued fraction

$$\Sigma^m_{1,N} = \frac{t^2_{1,2}}{\mu_2 - \Pi_{2,m} - \frac{t^2_{2,3}}{\mu_3 - \Pi_{3,m} \cdots - \frac{t^2_{N-1,N}}{\mu_N - \Pi_{N,m}}}}, \tag{10}$$

where $\Pi_{\ell m}$ denotes the sum of Coulomb energies due to interaction of an electron entering the ℓ-th QD with the other electrons present in the CCQD in configuration m. Note that in the uncorrelated limit ($U_\ell = 0$ and $U_{ij} = 0$), the above expressions reduce to the exact solution to the quantum transport through a linear chain within the nearest-neighbor tight-binding model.[16] Therefore, our results are still able to illustrate the transport behavior in the other extreme, $U/t_{ij} \ll 1$, since the terms we ignored are related to correlation of electrons in different levels, and it is valid when the Coulomb U terms become small. However, this study is restricted in the condition of $t_{i,j}/U \ll 1$ throughout article.

The average occupation numbers $N_{\ell,\sigma} = N_{\ell,\bar\sigma}$ and c_ℓ are determined by solving the on-site lesser Green's functions[12,13] $iG^<_{1,\sigma}(\epsilon)$, which take the following form

$$iG^<_{1,\sigma}(\epsilon) = 2\sum_m \frac{\Gamma_1(\epsilon) f_L + \Gamma^m_{1,N}(\epsilon) f_R}{\Gamma_1(\epsilon) + \Gamma^m_{1,N}(\epsilon)} Im G^r_{1,m}(\epsilon). \tag{11}$$

Thus, we have

$$N_1 = -\int \frac{d\epsilon}{\pi} \sum_m \frac{\Gamma_1(\epsilon) f_L + \Gamma^m_{1,N}(\epsilon) f_R}{\Gamma_1(\epsilon) + \Gamma^m_{1,N}(\epsilon)} Im G^r_{1,m}(\epsilon), \tag{12}$$

and

$$c_1 = -\int \frac{d\epsilon}{\pi} \sum_{m=4^{N-1}+1}^{2\times 4^{N-1}} \frac{\Gamma_1(\epsilon) f_L + \Gamma^m_{1,N}(\epsilon) f_R}{\Gamma_1(\epsilon) + \Gamma^m_{1,N}(\epsilon)} Im G^r_{1,m}(\epsilon), \tag{13}$$

where $\sum_{m=4^{N-1}+1}^{2\times 4^{N-1}}$ denotes a sum over configurations obtained by the product

$$N_{1\bar\sigma} \prod_{\ell=2}^{N} (a_\ell + b_{\ell,\sigma} + b_{\ell,\bar\sigma} + c_\ell) = \sum_{m=4^{N-1}+1}^{2\times 4^{N-1}} p_{1,m}. \tag{14}$$

To calculate the tunneling current from of Eq. (3), we also need the retarded Green's function $G^r_{1,\sigma}(\epsilon)$, which is given by $G^r_{1,\sigma}(\epsilon) = \sum_m G^r_{1,m}(\epsilon)$.

$N_{N,\sigma} = N_{N,\bar\sigma} = N_N$ and c_N have the same forms as the above equations with the indices 1 and N exchanged. $G^r_{N,m}(\epsilon)$ is obtained from $G^r_{1,m}(\epsilon)$ by reversing the roles of QDs 1 and N. Namely,

$$G^r_{N,m}(\epsilon) = p_{N,m}/(\mu_N - \Pi_{N,m} - \Sigma^m_{N,1}), \tag{15}$$

$$\Sigma^m_{N,1} = \frac{t^2_{N,N-1}}{\mu_{N-1} - \Pi_{N-1,m} - \frac{t^2_{N-1,N-2}}{\mu_{N-2} - \Pi_{N-2,m} \cdots - \frac{t^2_{2,1}}{\mu_1 - \Pi_{1,m}}}}, \tag{16}$$

and $p_{N,m}$ are determined by

$$(\bar{a}_N + \bar{b}_{N\bar\sigma}) \prod_{\ell=1}^{N-1} (a_\ell + b_{\ell\sigma} + b_{\ell,\bar\sigma} + c_\ell) = \sum_{m=1}^{2\times 4^{N-1}} p_{N,m}. \tag{17}$$

For QDs not in direct contact with leads (labeled by $\ell = 2, N-1$), we have

$$N_\ell = -\int \frac{d\epsilon}{\pi} \sum_{m=1}^{2\times 4^{N-1}} \frac{\Gamma^m_{\ell,1}(\epsilon) f_L + \Gamma^m_{\ell,N}(\epsilon) f_R}{\Gamma^m_{\ell,1}(\epsilon) + \Gamma^m_{\ell,N}(\epsilon)} Im G^r_{\ell,m}(\epsilon), \tag{18}$$

and

$$c_\ell = -\int \frac{d\epsilon}{\pi} \sum_{m=4^{N-1}+1}^{2\times 4^{N-1}} \frac{\Gamma^m_{\ell,1}(\epsilon) f_L + \Gamma^m_{\ell,N}(\epsilon) f_R}{\Gamma^m_{\ell,1}(\epsilon) + \Gamma^m_{\ell,N}(\epsilon)} Im G^r_{\ell,m}(\epsilon). \tag{19}$$

$\Gamma^m_{\ell,1}(\epsilon) = -2Im\Sigma^m_{\ell,1}$ and $\Gamma^m_{\ell,N}(\epsilon) = -2Im\Sigma^m_{\ell,N}$ are the effective tunneling rates for electrons from the ℓ-th QD to the left and right electrodes, respectively. The retarded Green's function $G^r_{\ell,m}(\epsilon)$ is given by

$$G^r_{\ell,m}(\epsilon) = \frac{p_{\ell,m}}{\mu_\ell - \Pi_{\ell,m} - \Sigma^m_{\ell,1} - \Sigma^m_{\ell,N}}, \tag{20}$$

where the probability factors, $p_{\ell,m}$ are determined by Eq. (9) with the indies 1 and ℓ interchanged. The self energies $\Sigma^m_{\ell,1}$ and $\Sigma^m_{\ell,N}$ are given by

$$\Sigma^m_{\ell,1} = \frac{t^2_{\ell,\ell-1}}{\mu_{\ell-1} - \Pi_{\ell-1,m} - \frac{t^2_{\ell-1,\ell-2}}{\mu_{\ell-2} - \Pi_{N-2,m} \cdots - \frac{t^2_{2,1}}{\mu_1 - \Pi_{1,m}}}} \tag{21}$$

and

$$\Sigma^m_{\ell,N} = \frac{t^2_{\ell,\ell+1}}{\mu_{\ell+1} - \Pi_{\ell+1,m} - \frac{t^2_{\ell+1,\ell+2}}{\mu_{\ell+2} - \Pi_{\ell+2,m} \cdots - \frac{t^2_{N-1,N}}{\mu_N - \Pi_{N,m}}}}. \tag{22}$$

The explicit expressions of $p_{\ell,m}$ and $\Pi_{\ell,m}$ for all levels and all configurations of the N=3 case are given in the Appendix. As an example, for a five-dot CCQD with configuration described by $p_{1,m} = a_1 b_{2\sigma} a_3 b_{4,\bar\sigma} c_5$, we have

$$G^r_{1,m}(\epsilon) =$$

$$\frac{(1-N_{1,\bar{\sigma}})b_{2\sigma}a_3b_{4,\bar{\sigma}}c_5}{\mu_1-U_{1,2}-\frac{t_{1,2}^2}{\mu_2-U_{1,2}-\frac{t_{2,3}^2}{\mu_3-U_{3,4}-\frac{t_{3,4}^2}{\mu_4-U_4-2U_{4,5}-\frac{t_{4,5}^2}{\mu_5-U_5-2U_{4,5}}}}}}. \tag{23}$$

In the linear response regime, Eqs. (5) and (6) can be rewritten as

$$J = \mathcal{L}_{11}\frac{\Delta V}{T}+\mathcal{L}_{12}\frac{\Delta T}{T^2} \tag{24}$$

$$Q = \mathcal{L}_{21}\frac{\Delta V}{T}+\mathcal{L}_{22}\frac{\Delta T}{T^2}, \tag{25}$$

where there are two sources of driving force to yield the charge and heat currents. $\Delta T = T_L - T_R$ is the temperature difference across the junction. Thermoelectric response functions $\mathcal{L}_{11}$, $\mathcal{L}_{12}$, $\mathcal{L}_{21}$, and $\mathcal{L}_{22}$ are evaluated by

$$\mathcal{L}_{11} = \frac{2e^2T}{h}\int d\epsilon\mathcal{T}(\epsilon)(\frac{\partial f(\epsilon)}{\partial E_F})_T, \tag{26}$$

$$\mathcal{L}_{12} = \frac{2eT^2}{h}\int d\epsilon\mathcal{T}(\epsilon)(\frac{\partial f(\epsilon)}{\partial T})_{E_F}, \tag{27}$$

$$\mathcal{L}_{21} = \frac{2eT}{h}\int d\epsilon\mathcal{T}(\epsilon)(\epsilon-E_F)(\frac{\partial f(\epsilon)}{\partial E_F})_T, \tag{28}$$

and

$$\mathcal{L}_{22} = \frac{2T^2}{h}\int d\epsilon\mathcal{T}(\epsilon)(\epsilon-E_F)(\frac{\partial f(\epsilon)}{\partial T})_{E_F}. \tag{29}$$

Here $\mathcal{T}(\epsilon)$ and $f(\epsilon) = 1/[e^{(\epsilon-E_F)/k_BT}+1]$ are evaluated under the equilibrium condition.

If the system is in an open circuit, the electrochemical potential will be established in response to a temperature gradient; this electrochemical potential is known as the Seebeck voltage (Seebeck effect). The Seebeck coefficient (amount of voltage generated per unit temperature gradient) is defined as $S = \Delta V/\Delta T = -\mathcal{L}_{12}/(T\mathcal{L}_{11})$. To judge whether the system is able to generate or extract heat efficiently, we need to consider the figure of merit,[1] which is given by

$$ZT = \frac{S^2G_eT}{\kappa_e+\kappa_{ph}} \equiv \frac{(ZT)_0}{1+\kappa_{ph}/\kappa_e}. \tag{30}$$

Here $G_e = \mathcal{L}_{11}/T$ is the electrical conductance and $\kappa_e = ((\mathcal{L}_{22}/T^2)-\mathcal{L}_{11}S^2)$ is the electron thermal conductance. $(ZT)_0$ represents the ZT value in the absence of phonon thermal conductance, κ_{ph}. For simplicity, we assume $\kappa_{ph} = \kappa_{ph,0}F_s$.[11–13] $\kappa_{ph,0} = \frac{\pi^2k_B^2T}{3h}$ is the universal phonon thermal conductance arising from acoustic phonon confinement in a nanowire,[17–19] which was confirmed in the phonon wave guide.[20] The expression of $\kappa_{ph} = \kappa_{ph,0}F_s$ with $F_s = 0.1$ can explain well the phonon thermal conductance of silicon nanowire with surface states calculated by the first-principles method.[17] The dimensionless scattering factor F_s arises from phonon scattering with surface impurities or surface defects of quantum dots.[1] It is possible to reduce phonon thermal conductance by one order of magnitude when the QD size is much smaller than the phonon mean free paths.[21,22] Therefore, we adopt $F_s = 0.01$ as a fixed parameter and assume F_s is independent of the number of QDs and QD size.

III. RESULTS AND DISCUSSION

A. Three-QD junction

In this section, we study the transport properties of N=3 case, which were experimentally[23,24] and theoretically[25,26] investigated in the nonlinear response regime to reveal the coherent and spin-dependent behavior of carrier transport. In Ref. [27], the Kondo transport of triple QDs was investigated by using the slave-boson method to remove the double occupation for each QD. This study is restricted in the Coulomb blockade regime. So far, few literatures have considered the spin-dependent thermoelectric properties of three coupled QDs. In Fig. 2 we plot the electrical conductance (G_e), Seebeck coefficient (S), and electron thermal conductance (κ_e) as a function of gate voltage for various temperatures. We adopt the following physical parameters $U_\ell = U_0 = 60\Gamma_0$, $U_{\ell,j} = 20\Gamma_0$, $t_{\ell,j} = 1\Gamma_0$, $\Gamma_1 = \Gamma_3 = \Gamma = \Gamma_0$, $E_1 = E_2 = E_F - 20\Gamma_0$, and $E_3 = E_F + 30\Gamma_0 - eV_g$. All energy scales are in units of Γ_0, a characteristic energy. A gate voltage is applied to tune the energy level of E_3 such that the E_3 level can be varied from being empty to singly occupied (see the inset of Fig.2). The system with spin triple state as illustrated in the inset of Fig. 2(a) is in the insulating state when E_3 is far above the Fermi energy. The conductance G_e reaches a maximum at $E_3 = E_F$, whose magnitude decreases as the temperature increases. Meanwhile, G_e a a function of V_g has a Lorentz shape, whose FWHM is almost independent of temperature as long as $k_BT/\Gamma \geq 1$. This is referred to as the nonthermal broadening effect, which was also observed in the case of serially coupled quantum dots (SCQD).[12,28] The behavior of Seebeck coefficient (S) is illustrated in Fig. 2(b), and it is found that S vanishes when G_e reaches the maximum, a result attributed to the electron-hole symmetry. Here, holes are defined as missing electrons in electrodes below E_F. The negative sign of S indicates that electrons are majority carries, which diffuse to the right electrode from the left electrode through energy levels above E_F. On the other hand, holes become majority carriers when S turns positive. Thus, the measurement of S can reveal the properties of resonant channels when compared with that of G_e. We see that S vanishes again at $k_BT = 1\Gamma_0$

and $eV_g = 50\Gamma_0$, where $E_3 + U_J$ is lined up with E_F. The behavior of electron thermal conductance κ_e is similar to that of G_e and also shows the nonthermal broadening effect. Like the two-QD junction, the nonthermal broadening effect of the three-QD junction can be used to function as a low temperature filter.

In Fig. 3, we show thermoelectric behaviors of a system with $E_1 = E_F - 20\Gamma_0$, $E_2 = E_F + 10\Gamma_0 - eV_g$, and $E_3 = E_F$, as illustrated in the inset of Fig. 3(a). Other physical parameters are the same as those of Fig. 2. Now the gate voltage is used to tune the level E_2 such that the E_2 level varies from being empty to singly occupied. Meanwhile, the E_3 level will be depleted when E_2 is singly occupied. Although the behavior of G_e shown in Fig. 3(a) is very similar to that of Fig. 2(a), we note the FWHM of G_e in Fig. 3(a) is nearly twice as large. Furthermore, the nonthermal broadening effect for κ_e disappears. This indicates that the "effective broadening" of energy level of dot 2, which is not directly coupled to electrodes, is different from that of dots 1 and 3. The nonthermal broadening effect of G_e is an essential characteristic of resonant junction system. Once k_BT is larger than the tunneling rates $\Gamma_1 = \Gamma_3 = \Gamma$, which is the broadening of energy levels of dots 1 and 3, the broadening of G_e depends mainly on the lifetime of the resonance, and becomes insensitive to the temperature factor $1/\cosh^2((\epsilon - E_F)/(2k_BT))$. In addition, we find more oscillatory peaks of S in Fig. 3(b) as compared in Fig. 2(b). For example, when $eV_g = 10\Gamma_0$ we have $E_2 = E_F$, which matches with E_3 and $E_1 + U_I$. This resonance has very small probability weight and is non-observable in G_E, whereas it can be measured by S. The highly oscillatory behavior of S with respect to V_g indicates that carriers with high energies can diffuse to the right electrode through more resonant channels, which are far above E_F. This explains why the tail of κ_e peak (near $eV_g = 20\Gamma_0$ and $eV_g = 40\Gamma_0$) increases with increasing temperature.

In Fig. 4, we plot the average occupation number N_ℓ, G_e and S as functions of the gate voltage V_g (which is used to tune E_2) for various temperatures for a three-QD junction system in the spin-blockade configuration, as illustrated in the inset of Fig. 4(b). Here, $E_1 = E_F - 10\Gamma_0$, $E_2 = E_F + 10\Gamma_0 - eV_g$, $E_3 = E_F - 60\Gamma_0$, and $U_{\ell,j} = 10\Gamma_0$. Other physical parameters are the same as those of Fig. 3. This configuration was considered in Ref. [26] within the framework of Master equation technique for studying spin-blockade behavior of three coupled QD in the nonlinear response regime. A spin-blockade can occur, because the second electron appears in dot 3 must satisfy the Pauli exclusion principle. As seen in Fig. 4(a), the E_2 level is tuned from being empty to singly occupied, while the E_3 level remains singly occupied even in presence of the interdot Coulomb interactions. We observe a small bump of G_e near $eV_g = 20\Gamma_0$. Although both E_1 and E_2 become resonant at $eV_g = 20\Gamma_0$, electrons in this resonance state can not tunnel to the right electrode through E_3, due to the presence of U_J arising in dot 3. The maximum G_e occuring at $eV_g = 30\Gamma_0$ is resulting from the resonance: $E_1 + U_I = E_2 + U_I + U_J = E_3 + U_3$ (described by $p_{1,10}$), which is the Pauli spin blockade process for the case of three-QD junction. The maximum G_e in this spin singlet state is small than the maximum of G_e in spin triple state of Fig. 2. From the results of Figs. (2)-(4), we find that the maximum Seebeck coefficients are smaller than one. This is not preferred for the purpose of enhancing ZT. Such a result also implies that the fluctuation of QD energy levels in CCQD will suppress ZT.

In Fig. 5, we plot the occupation numbers N_ℓ, electrical conductance G_e, Seebeck coefficient S, and electron thermal conductance κ_e as functions of gate voltage at $k_BT = 1\Gamma_0$. We consider identical energy levels with $E_\ell = E_0 = E_F + 30\Gamma_0 - eV_g$ and $t_{\ell,j} = 6\Gamma_0$. All QD levels are tuned by the gate voltage from far above E_F to far below E_F. Other physical parameters are the same as those of Fig. 2. Because $t_{\ell,j} = t_c > k_BT$ and $t_{\ell,j} = t_c > \Gamma$, these thermal response functions (G_e, S, and κ_e) display structures yielded by the electron hopping effect. The three peaks labeled by V_{g1}, V_{g2}, and V_{g3} correspond to three resonant channels at $E_0 - \sqrt{2}\, t_c$, E_0, and $E_0 + \sqrt{2}\, t_c$, which are poles of the Green's function $G^r_{1,m}(\epsilon)$ for channel $m = 1$, in which all three QDs are empty. The strengths of these peaks are determined by their probability weights, $\bar{a}_1 a_2 a_3$. Another three peaks labeled by V_{g4}, V_{g5}, and V_{g6} result from the resonances corresponding to channel $m = 28$ with $p_{1,m} = N_{1\bar{\sigma}} b_{2\sigma} c_3$, in which dots 1 and 3 are doubly occupied and dot 2 occupied with one electron with spin σ. (see Appendix) A remarkable result of Fig. 5 is the larger enhancement of the maximum Seebeck coefficient. This enhancement of the maximum S is due to the degeneracy of QD levels, instead from larger t_c. Note that S is sensitive to the fluctuation of QD energy levels, but not to t_c.[13] This will be further demonstrated in the $N = 5$ case. Unlike two-QD junction with identical QDs, the spectra of these thermal response functions for the three-QD junction do not possess symmetric behavior as a result of the interdot Coulomb interactions. The central dot (dot 2) feels the Coulomb interactions from both dots 1 and 2, while dots 1 and 3 can only feel the interdot Coulomb interaction from the central dot. Such an effect can be observed in the behaviors of occupation numbers as functions of eV_g.

The electrical conductance G_e, Seebeck coefficient S, and figure of merit ZT are plotted as functions of detuning energy $\Delta = E_\ell - E_F$ with and without interdot Coulomb interaction at $k_BT = 10\Gamma_0$ in Fig. 6, where we have adopted $t_{\ell,j} = 6\Gamma_0$ and $\Gamma_l = \Gamma_R = \Gamma_0$. We note G_e is suppressed by the interdot Coulomb interactions. Such an effect becomes weak, when Δ increases. S is almost independent of $U_{\ell,j}$ and it shows a linear dependence of Δ, roughly described by $-k_B\Delta/(eT)$. The behavior of ZT as a function of Δ can be described by the function ZT$= \alpha\Delta^2/(T^3 cosh^2(\Delta/2k_BT))$, where α is independent of T and Δ. When $\Delta \gg k_BT$, κ_e becomes negligible. Therefore, the thermal conductance is dominated by κ_{th}, which is assumed to be a linear function of T. ZT is determined by the power factor of S^2G_e. The maximum

ZT occurs near $\Delta_{max} = 3k_BT$ and it is slightly reduced in the presence of $U_{\ell,j}$. The effect of $U_{\ell,j}$ becomes negligible when the QD energy levels are far above E_F. In the following discussion, we will show that electron Coulomb interactions are important when E_F is above E_ℓ.

Fig. 7 shows G_e, S, and ZT as functions of gate voltage at $k_BT = 10\Gamma_0$ and $E_\ell = E_0 = E_F + 50\Gamma_0 - eV_g$ for various interdot Coulomb interactions. Other physical parameters are the same as those of Fig. 3. Comparing with the low-temperature results given in Fig. 5, we see that the six peaks of G_e at $k_BT = 1\Gamma_0$ now become two broad peaks. We also note that the presence of interdot Coulomb interactions breaks the structure symmetry (taking $eV_g = 80\Gamma_0$ as the mid pint, where E_F sits between E_ℓ and $E_\ell + U_\ell$ with equal separation). In particular, $ZT_{max,>}$ (for QD energy levels above E_F) is only slightly suppressed with increasing interdot Coulomb interactions. On the other hand, $ZT_{max,<}$ (for QD energy levels below E_F) is significantly suppressed. The difference in interdot Coulomb interactions between central dot and two outer dots leads to an artificial "QD energy level fluctuation" which suppresses ZT. Our result indicates that the optimization of ZT prefers having the QD levels above E_F, although many studies of individual QDs and two coupled QDs indicated that electron Coulomb interactions can enhance ZT when QD levels are below E_F.[29−32] Authors in reference[29-32] adopted the mean field approximation, which truncates the high order Green's functions arising from electron Coulomb interactions.

B. Effect of number of QDs in CCQD

Since in realistic QD junctions for thermoelectric application, one needs to consider a large number of serially coupled QDs in order to accommodate reasonable temperature gradient across the junction, it is important to know the effect of number of QDs (N) on the thermoelectric properties of a CCQD system for a given t_c. To clarify the effect of N on ZT, we plot G_e, S, κ_e, and ZT as functions of temperature for various values of N by using the following physical parameters: $E_\ell = E_0 = E_F + 30\Gamma_0$, $U_\ell = U_0 = 30\Gamma_0$, $t_c = 3\Gamma_0$. The interdot Coulomb interactions have been turned off. Increasing the number of QDs would change the density of states (DOS) of the CCQD system from atomic limit to the band limit. For N varying from 2 to 5, in the absence of electron Coulomb interactions, we have the following energy spectra (under the condition $t_c/\Gamma \gg 1$)

$$N = 2 : \epsilon = E_0 + t_c,\ E_0 - t_c;$$

$$N = 3 : \epsilon = E_0 + \sqrt{2}t_c, E_0,\ E_0 - \sqrt{2}t_c;$$

$$N = 4 : \epsilon = E_0 + \sqrt{(3+\sqrt{5})/2}\ t_c,\ E_0 + \sqrt{(3-\sqrt{5})/2}\ t_c,$$

$$E_0 - \sqrt{(3-\sqrt{5})/2}\ t_c,\ E_0 - \sqrt{(3+\sqrt{5})/2}\ t_c;$$

$$N = 5 : \epsilon = E_0 + \sqrt{3}t_c,\ E_0 + t_c,\ E_0,$$

$$E_0 - t_c,\ E_0 - \sqrt{3}t_c.$$

The separations between these resonant channels become small with increasing QD numbers. In addition, these resonant channels have different broadening. For example, three resonant channels of the $N = 3$ case occur at $\epsilon = E_0 + \sqrt{2}t_c$, E_0, and $E_0 - \sqrt{2}t_c$, and their broadening widths are $\Gamma/4$, $\Gamma/2$, and $\Gamma/4$, respectively. As expected, the maximum ZT decreases with increasing N. Based on the results of Fig. 8, the reduction of maximum ZT is attributed to the reduction of G_e. Increasing N, the resonant channels increases whereas probability weights of these resonant channels decrease. This explains why G_e is reduced with increasing N. Note that when Coulomb interactions are turned off, G_e would become insensitive to N for the case of small t_c and large $\Delta = E_\ell - E_F$. The larger t_c, the more important the QD number effect becomes. In the high temperature regime, we find that the Seebeck coefficient is not sensitive to N [see Fig. 8(b)], while k_e reduces significantly as N increases [see Fig. 8(c)]. Thus, k_{ph} dominates the thermal conductance in the large N limit. Consequently, the behavior of ZT is essentially determined by the power factor ($pF = S^2G_e$), and the trend of ZT with respect to increasing N is similar to that of G_e. We also note that the dependence of all thermoelectric functions on N saturates once N reaches 5 for the weak hopping strength considered, $t_c = 3\Gamma_0$. Thus, it is sufficient to model the thermoelectric behaviors of a CCQD with large N by using $N = 5$. However, for larger t_c, the saturation behavior would occur at larger N.

In order to find the optimization condition of ZT, we plot in Fig. 9 the occupation number of each QD, electrical conductance, Seebeck coefficient, and ZT as functions of gate voltage for various temperatures for a 5-dot CCQD. Other physical parameters are the same as the $N = 5$ case shown in Fig. 8. From Fig. 9(a) we see a small difference in the occupation number between exterior dots (N_1, N_5) and interior dots (N_2, N_3, N_4) even though the interdot Coulomb interactions are turned off. This phenomena also occurs in the $N = 3$ and $N = 4$ cases (not shown here). The occupation number fluctuation was also reported in Ref. [25] for the $N = 3$ case by solving the Master equation. For $eV_g = 25\Gamma_0$, electrons prefer to occupy the outer QDs (N_1 and N_5). For $eV_g = 75\Gamma_0$, electrons prefer to accumulate in the interior QDs (N_2, N_3, N_4). The maximum electrical conductance is suppressed with increasing temperature, while the peak width becomes wider. Such a behavior is no different from a single QD with multiple energy levels.[11] However, we note that $G_{e,max}$ does not have a Lorentzian shape even though each resonant channel has a Lorentzian shape. This is mainly attributed to the formation of a "miniband" with the probability weight $(1-N_{1,\bar{\sigma}})(1-N_{2\bar{\sigma}})(1-N_{3,\bar{\sigma}})(1-N_{4,\bar{\sigma}})(1-N_{5,\bar{\sigma}})$. Note that once $U_{\ell,j}=0$, there are only two kind of probability weights $(1-N_{\ell,\bar{\sigma}})$ and $N_{\ell,\bar{\sigma}}$ for each QD.[33]This characteristic can also be demonstrated from the expressions for N=3 given in the appendix. When the applied gate voltage continue to increase, the CCQD turns into a Mott-insulator at half-filling $N_\ell = N_{\ell,\sigma} = N_{\ell,\bar{\sigma}} = 0.5$, resulting from Coulomb band gap.[33] (The electrical conductance almost vanishes for each QD with one electron). The upper "miniband" with probability weight $N_{1,\bar{\sigma}}N_{2\bar{\sigma}}N_{3,\bar{\sigma}}N_{4,\bar{\sigma}}N_{5,\bar{\sigma}}$ arises for electrons hopping between energy levels at E_0+U_0. The Seebeck coefficient shown in Fig. 9(c) goes through zero at V_{g1}, V_{g2}, and V_{g3}, respectively. At these applied gate voltages, the CCQD has an electron-hole symmetry. Note that the Seebeck coefficient vanishes at the half-filling case. We see that the electrical conductance and Seebeck coefficient are very sensitive to QD energy levels. Due to the electron-hole symmetry, the G_e and ZT curves are symmetric (while S curve is antisymmetric) with respect to the mid point at $eV_g = 45\Gamma_0$. Thus, ZT curve has two maxima, one for QD energy levels above E_F and the other for QD energy levels below E_F. The maximum ZT at $k_BT = 5\Gamma_0$ can reach 8 for V_g near $10\Gamma_0$ and $80\Gamma_0$. When κ_{ph} dominates the thermal conductance, the maximum ZT values are correlated to the maximum power factor. The maximum ZT occurs at neither good conducting state nor insulating state, because the maximum G_e (good conductance)is accompanied by a poor Seebeck coefficient, and vice versa. Note that the results shown in Fig. 9 are for the case with no interdot Coulomb interactions, i.e. $U_{\ell,j}=0$. Once $U_{\ell,j}$ are turned on, the spectra of G_e becomes somewhat complicated to analyze. Meanwhile, it would significantly lower the maximum ZT value for the peak with $E_F > E_0$.

Electron interdot hopping strength t_c is a key parameter in determining the bandwidth of the miniband, which would affect the thermoelectric properties. Fig. 10 shows G_e, S, $(ZT)_0$ and ZT as functions of t_c for various detuning energies $\Delta = E_\ell - E_F$ at $k_BT = 10\Gamma_0$. Here, we consider the case with on-site Coulomb interaction $U = 60\Gamma_0$ and zero interdot Coulomb interaction. Note that $(ZT)_0$ corresponds to ZT in the absence of phonon thermal conductance. When t_c is smaller than Γ_0, G_e increases quickly with respect to t_c. This behavior can be explained by the fact of that the transmission factor is proportional to t_c^8 for the 5-dot case when t_c approaches zero. Once t_c is larger than Γ_0, G_e becomes almost saturated. G_e values at $\Delta = 10\Gamma_0$ are very close to those at $\Delta = 20\Gamma_0$. Such a behavior is also seen in the dotted line of Fig. 9(b), in which the QD energy level is tuned by the gate voltage. We notice that S is rather insensitive to t_c in the weak hoping limit, $t_c/\Gamma_0 \ll 1$ ($S \approx -k_B\Delta/eT$). In the absence of phonon thermal conductance, $(ZT)_0$ diverges in the weak hoping limit, because the Lorenz number $L = \kappa_e/(G_eT)$ approaches zero. From Fig. 10(d), we see that ZT increases with increasing t_C, reaching an optimum value at $t_C \approx 2\Gamma_0$ and then decreases for higher t_c. The reduction of ZT at higher t_c arises from the faster reduction of S^2 in comparison with the increase of G_e. To reveal how the asymmetrical coupling between the QDs and the electrodes influences ZT, we also plot ZT versus V_g for the detuning energy $\Delta = 30\Gamma_0$ for different tunneling rates in Fig. 10(d). (See curves marked by filled triangles and diamonds) The maximum ZT is suppressed when the ratio of Γ_L/Γ_R is far away from 1, while keeping the same average value, $\Gamma_L + \Gamma_R = 2\Gamma_0$.

IV. SUMMARY AND CONCLUSIONS

In summary, we have theoretically investigated the thermoelectric effects of CCQD embedded in a nanowire and connected to metallic electrodes. The length of the CCQD nanowire is finite, and shorter than the electron mean free path. Thus, the electron-phonon interaction effect can be ignored in this study. We have derived an expression for the transmission coefficient $\mathcal{T}(\epsilon)$ in terms of the on-site retarded Green's functions and effective tunneling rates involving electron hopping and Coulomb interactions, which keeps the same form as the Landauer formula for charge and heat currents. Closed-form expressions (which are correct in the limit $t_{ij}/U \ll 1$) for the retarded Green's functions of a CCQD system with arbitrary number of QDs are derived. Such an analytical form is quite needed for finding the best ZT values. In addition, our formula still works in the nonequilibrium regime.

In the linear response regime, electrical conductance G_e, Seebeck coefficient S, electron thermal conductance κ_e, and figure of merit ZT are calculated for finite length CCQDs with QD number ranging from 2 to 5. The thermoelectric properties of spin-dependent configurations (spin triple and singlet states) are studied. The nonthermal broadening behavior of G_e is maintained in the three-QD case in the presence of electron Coulomb interactions, because such a behavior is the essential feature of resonant tunneling junction system.[12,28] Note that the nonthermal broadening effect of G_e can not be illustrated by using the mean-field approximation.[30−32] When QDs are not identical, these thermoelectric response functions are weaker, resulting from symmetry breaking in the junction structure. Unlike the case of double QDs,[10] the interdot Coulomb interactions lead to considerable suppression of the maximum ZT value in the three-QD case when the degenerate QD energy levels are below E_F. This is caused by the symmetry breaking via interdot Coulomb interactions in the CCQD junction.

We find that for a given t_c, increasing the QD number N in the CCQD would suppress the maximum ZT value, and the reduction quickly saturates once N reaches 5 in the weak hopping limit ($t_c/U \ll 1$). However, for larger t_c, the saturation behavior would occur at larger N. In addition, we illustrate that the QD energy level fluctuation suppresses the maximum ZT by using a three-QD junction. We find that the Seebeck coefficient is insensitive to t_c and $U_\ell(U_{\ell,j})$ when QD energy levels are far above E_F, and it can be approximated by a simple linear expression, $S = -k_B\Delta/eT$, where $\Delta = E_\ell - E_F$ and T is the equilibrium temperature. This characteristic of $S = -k_B\Delta/eT$ was also reported in an infinite Hubbard chain with narrow bandwidth.[34−36] The feature of $S = \Delta V/\Delta T \approx -k_B\Delta/eT$ can be utilized to realize a temperature sensor.[37] Therefore, the CCQD system is more promising than the single QD junction for measurement of larger temperature difference.

Acknowledgment
This work was supported in part by National Science Council, Taiwan under Contract Nos. NSC 101-2112-M-008-014-MY2 and NSC 101-2112-M-001-024-MY3.

† E-mail address: mtkuo@ee.ncu.edu.tw
* E-mail address: yiachang@gate.sinica.edu.tw

Appendix A: Green's functions of N=3

In this appendix, we give the detailed expression of $\mathcal{T}_{1,3}$ for the N=3 case. For simplicity, we assume the same interdot hopping constant between any two QDs, i.e. $t_{\ell,j} = t_c$, and we denote $U_{1,2} = U_{2,1} \equiv U_I$, $U_{2,3} = U_{3,2} \equiv U_J$, and $\mu_\ell = \epsilon - E_\ell + i\Gamma_\ell/2$; $\ell = 1,2,3$. Note that $\Gamma_2 = 0$, because QD 2 is not directly coupled to the electrodes. Eq. (5) becomes

$$\mathcal{T}_{1,3}(\epsilon) = -2\sum_{m=1}^{32} \frac{\Gamma_1(\epsilon)\Gamma^m_{1,3}(\epsilon)}{\Gamma_1(\epsilon) + \Gamma^m_{1,3}(\epsilon)} \mathrm{Im} G^r_{1,m}(\epsilon), \tag{A1}$$

where

$$G^r_{1,m}(\epsilon) = \frac{p_{1,m}}{\mu_1 - \Pi_{1,m} - \Sigma^m_{1,3}}, \tag{A2}$$

$$\Sigma^m_{1,3} = \frac{t_c^2}{\mu_2 - \Pi_{2,m} - \frac{t_c^2}{\mu_3 - \Pi_{3,m}}}, \tag{A3}$$

and $\Gamma^m_{1,3} = -2Im\Sigma^m_{1,3}$ denotes the effective tunneling rate of the electron from the first QD energy level to the right electrode via channel m. The probability weights ($p_{1,m}$) and Coulomb energies ($\Pi_{\ell,m}$) are given by

$$p_{1,1} = \bar{a}_1 a_2 a_3; \Pi_{1,1} = \Pi_{2,1} = \Pi_{3,1} = 0.$$

$$p_{1,2} = \bar{a}_1 a_2 b_{3,\bar{\sigma}}; \Pi_{1,2} = 0, \Pi_{2,2} = U_J, \Pi_{3,2} = U_3.$$

$$p_{1,3} = \bar{a}_1 a_2 b_{3,\sigma}; \Pi_{1,3} = 0, \Pi_{2,3} = \Pi_{3,3} = U_J.$$

$$p_{1,4} = \bar{a}_1 a_2 c_3; \Pi_{1,4} = 0, \Pi_{2,4} = 2U_J, \Pi_{3,4} = U_3 + U_J.$$

$$p_{1,5} = \bar{a}_1 b_{2,\bar{\sigma}} a_3; \Pi_{1,5} = U_I, \Pi_{2,5} = U_2, \Pi_{3,5} = U_J.$$

$$p_{1,6} = \bar{a}_1 b_{2,\bar{\sigma}} b_{3,\bar{\sigma}}; \Pi_{1,6} = U_I, \Pi_{2,6} = U_2 + U_J, \Pi_{3,6} = U_3 + U_J.$$

$$p_{1,7} = \bar{a}_1 b_{2,\bar{\sigma}} b_{3,\sigma}; \Pi_{1,7} = U_I, \Pi_{2,7} = U_2 + U_J, \Pi_{3,7} = 2U_J.$$

$$p_{1,8} = \bar{a}_1 b_{2,\bar{\sigma}} c_3; \Pi_{1,8} = U_I, \Pi_{2,8} = U_2 + 2U_J, \Pi_{3,8} = U_3 + 2U_J.$$

$$p_{1,9} = \bar{a}_1 b_{2,\sigma} a_3; \Pi_{1,9} = U_I, \Pi_{2,9} = U_I, \Pi_{3,9} = 0.$$

$$p_{1,10} = \bar{a}_1 b_{2,\sigma} b_{3,\bar{\sigma}}; \Pi_{1,10} = U_I, \Pi_{2,10} = U_I + U_J, \Pi_{3,10} = U_3.$$

$$p_{1,11} = \bar{a}_1 b_{2,\sigma} b_{3,\sigma}; \Pi_{1,11} = U_I, \Pi_{2,11} = U_I + U_J, \Pi_{3,11} = U_J.$$

$$p_{1,12} = \bar{a}_1 b_{2,\sigma} c_3; \Pi_{1,12} = U_I, \Pi_{2,12} = U_I + 2U_J, \Pi_{3,12} = U_3 + U_J.$$

$$p_{1,13} = \bar{a}_1 c_2 a_3; \Pi_{1,13} = 2U_I, \Pi_{2,13} = U_2 + U_I, \Pi_{3,13} = U_J.$$

$$p_{1,14} = \bar{a}_1 c_2 b_{3,\bar{\sigma}};$$

$$\Pi_{1,14} = 2U_I, \Pi_{2,14} = U_2 + U_I + U_J, \Pi_{3,14} = U_3 + U_J.$$

$$p_{1,15} = \bar{a}_1 c_2 b_{3,\sigma};$$

$$\Pi_{1,15} = 2U_I, \Pi_{2,15} = U_2 + U_I + U_J, \Pi_{3,15} = 2U_J.$$

$$p_{1,16} = \bar{a}_1 c_2 c_3;$$

$$\Pi_{1,16} = 2U_I, \Pi_{2,16} = U_2 + U_I + 2U_J, \Pi_{3,16} = U_3 + 2U_J.$$

$$p_{1,17} = N_{1,\bar{\sigma}} a_2 a_3; \Pi_{1,17} = U_1, \Pi_{2,17} = U_I, \Pi_{3,17} = 0.$$

$$p_{1,18} = N_{1,\bar{\sigma}} a_2 b_{3,\bar{\sigma}}; \Pi_{1,18} = U_1, \Pi_{2,18} = U_I + U_J, \Pi_{3,18} = U_3.$$

$$p_{1,19} = N_{1,\bar{\sigma}} a_2 b_{3,\sigma}; \Pi_{1,19} = U_1, \Pi_{2,19} = U_I + U_J, \Pi_{3,19} = U_J.$$

$$p_{1,20} = N_{1,\bar{\sigma}} a_2 c_3;$$

$$\Pi_{1,20} = U_1, \Pi_{2,20} = U_I + 2U_J, \Pi_{3,20} = U_3 + U_J.$$

$$p_{1,21} = N_{1,\bar{\sigma}} b_{2,\bar{\sigma}} a_3;$$

$$\Pi_{1,21} = U_1 + U_I, \Pi_{2,21} = U_2 + U_I, \Pi_{3,21} = U_J.$$

$$p_{1,22} = N_{1,\bar{\sigma}} b_{2,\bar{\sigma}} b_{3,\bar{\sigma}};$$

$$\Pi_{1,22} = U_1 + U_I, \Pi_{2,22} = U_2 + U_I + U_J, \Pi_{3,22} = U_3 + U_J.$$

$$p_{1,23} = N_{1,\bar{\sigma}} b_{2,\bar{\sigma}} b_{3,\sigma};$$

$$\Pi_{1,23} = U_1 + U_I, \Pi_{2,23} = U_2 + U_I + U_J, \Pi_{3,23} = 2U_J.$$

$$p_{1,24} = N_{1,\bar{\sigma}} b_{2,\bar{\sigma}} c_3;$$

$$\Pi_{1,24} = U_1 + U_I, \Pi_{2,24} = U_2 + U_I + 2U_J, \Pi_{3,24} = U_3 + 2U_J.$$

$$p_{1,25} = N_{1,\bar{\sigma}} b_{2,\sigma} a_3;$$

$$\Pi_{1,25} = U_1 + U_I, \Pi_{2,25} = 2U_I, \Pi_{3,25} = 0.$$

$$p_{1,26} = N_{1,\bar{\sigma}} b_{2,\sigma} b_{3,\bar{\sigma}};$$

$$\Pi_{1,26} = U_1 + U_I, \Pi_{2,26} = 2U_I + U_J, \Pi_{3,26} = U_3.$$

$$p_{1,27} = N_{1,\bar{\sigma}} b_{2,\sigma} b_{3,\sigma};$$

$$\Pi_{1,27} = U_1 + U_I, \Pi_{2,27} = 2U_I + U_J, \Pi_{3,27} = U_J.$$

$$p_{1,28} = N_{1,\bar{\sigma}} b_{2,\sigma} c_3;$$

$$\Pi_{1,28} = U_1 + U_I, \Pi_{2,28} = 2U_I + 2U_J, \Pi_{3,28} = U_3 + U_J.$$

$$p_{1,29} = N_{1,\bar{\sigma}} c_2 a_3;$$

$$\Pi_{1,29} = U_1 + 2U_I, \Pi_{2,29} = U_2 + 2U_I, \Pi_{3,29} = U_J.$$

$$p_{1,30} = N_{1,\bar{\sigma}} c_2 b_{3,\bar{\sigma}};$$

$$\Pi_{1,30} = U_1 + 2U_I, \Pi_{2,30} = U_2 + 2U_I + U_J, \Pi_{3,30} = U_3 + U_J.$$

$$p_{1,31} = N_{1,\bar{\sigma}} c_2 b_{3,\sigma};$$

$$\Pi_{1,31} = U_1 + 2U_I, \Pi_{2,31} = U_2 + 2U_I + U_J, \Pi_{3,31} = 2U_J.$$

$$p_{1,32} = N_{1,\bar{\sigma}} c_2 c_3;$$

$$\Pi_{1,32} = U_1 + 2U_I, \Pi_{2,32} = U_2 + 2U_I + 2U_J, \Pi_{3,32} = U_3 + 2U_J.$$

For the retarded Green's unction of QD 2, we have

$$G^r_{2,m}(\epsilon) \;=\; \frac{p_{2,m}}{\mu_2 - \Pi_{2,m} - \Sigma^m_{2,1} - \Sigma^m_{2,3}}, \qquad \text{(A4)}$$

where $\Sigma^m_{2,1} = \frac{t_c^2}{\mu_1 - \Pi_{1,m}}$ and $\Sigma^m_{2,3} = \frac{t_c^2}{\mu_3 - \Pi_{3,m}}$. The probability factors, $p_{2,m}$ and Coulomb energies $\Pi_{\ell,m}; \ell = 1,2,3$ are given by

$$p_{2,1} = \bar{a}_2 a_1 a_3; \Pi_{1,1} = \Pi_{2,1} = \Pi_{3,1} = 0.$$

$$p_{2,2} = \bar{a}_2 a_1 b_{3,\bar{\sigma}}; \Pi_{1,2} = 0, \Pi_{2,2} = U_J, \Pi_{3,2} = U_3.$$

$$p_{2,3} = \bar{a}_2 a_1 b_{3,\sigma}; \Pi_{1,3} = 0, \Pi_{2,3} = \Pi_{3,3} = U_J.$$

$$p_{2,4} = \bar{a}_2 a_1 c_3; \Pi_{1,4} = 0, \Pi_{2,4} = 2U_J, \Pi_{3,4} = U_3 + U_J.$$

$$p_{2,5} = \bar{a}_2 b_{1,\bar{\sigma}} a_3; \Pi_{1,5} = U_1, \Pi_{2,5} = U_I, \Pi_{3,5} = 0.$$

$$p_{2,6} = \bar{a}_2 b_{1,\bar{\sigma}} b_{3,\bar{\sigma}}; \Pi_{1,6} = U_1, \Pi_{2,6} = U_I + U_J, \Pi_{3,6} = U_3.$$

$$p_{2,7} = \bar{a}_2 b_{1,\bar{\sigma}} b_{3,\sigma}; \Pi_{1,7} = U_1, \Pi_{2,7} = U_I + U_J, \Pi_{3,7} = U_J.$$

$$p_{2,8} = \bar{a}_2 b_{1,\bar{\sigma}} c_3; \Pi_{1,8} = U_1, \Pi_{2,8} = U_I + 2U_J, \Pi_{3,8} = U_3 + U_J.$$

$$p_{2,9} = \bar{a}_2 b_{1,\sigma} a_3; \Pi_{1,9} = U_I, \Pi_{2,9} = U_I, \Pi_{3,9} = 0.$$

$$p_{2,10} = \bar{a}_2 b_{1,\sigma} b_{3,\bar{\sigma}}; \Pi_{1,10} = U_I, \Pi_{2,10} = U_I + U_J, \Pi_{3,10} = U_3.$$

$$p_{2,11} = \bar{a}_2 b_{1,\sigma} b_{3,\sigma}; \Pi_{1,11} = U_I, \Pi_{2,11} = U_I + U_J, \Pi_{3,11} = U_J.$$

$$p_{2,12} = \bar{a}_2 b_{1,\sigma} c_3; \Pi_{1,12} = U_I, \Pi_{2,12} = U_I + 2U_J, \Pi_{3,12} = U_3 + U_J.$$

$$p_{2,13} = \bar{a}_2 c_1 a_3; \Pi_{1,13} = U_1 + U_I, \Pi_{2,13} = 2U_I, \Pi_{3,13} = 0.$$

$$p_{2,14} = \bar{a}_2 c_1 b_{3,\bar{\sigma}};$$

$$\Pi_{1,14} = U_1 + U_I, \Pi_{2,14} = 2U_I + U_J, \Pi_{3,14} = U_3.$$

$$p_{2,15} = \bar{a}_2 c_1 b_{3,\sigma};$$

$$\Pi_{1,15} = U_1 + U_I, \Pi_{2,15} = 2U_I + U_J, \Pi_{3,15} = U_J.$$

$$p_{2,16} = \bar{a}_2 c_1 c_3;$$

$$\Pi_{1,16} = U_1 + U_I, \Pi_{2,16} = 2U_I + 2U_J, \Pi_{3,16} = U_3 + U_J.$$

$$p_{2,17} = N_{2,\bar{\sigma}} a_1 a_3; \Pi_{1,17} = U_I, \Pi_{2,17} = U_2, \Pi_{3,17} = U_J.$$

$$p_{2,18} = N_{2,\bar{\sigma}} a_1 b_{3,\bar{\sigma}}; \Pi_{1,18} = U_I, \Pi_{2,18} = U_2 + U_J, \Pi_{3,18} = U_3 + U_J.$$

$$p_{2,19}=N_{2,\bar{\sigma}}a_1b_{3,\sigma};\Pi_{1,19}=U_I,\Pi_{2,19}=U_2+U_J,\Pi_{3,19}=2U_J.$$

$$p_{2,20}=N_{2,\bar{\sigma}}a_1c_3;$$

$$\Pi_{1,20}=U_I,\Pi_{2,20}=U_2+2U_J,\Pi_{3,20}=U_3+2U_J.$$

$$p_{2,21}=N_{2,\bar{\sigma}}b_{1,\bar{\sigma}}a_3;$$

$$\Pi_{1,21}=U_1+U_I,\Pi_{2,21}=U_2+U_I,\Pi_{3,21}=U_J.$$

$$p_{2,22}=N_{2,\bar{\sigma}}b_{1,\bar{\sigma}}b_{3,\bar{\sigma}};$$

$$\Pi_{1,22}=U_1+U_I,\Pi_{2,22}=U_2+U_I+U_J,\Pi_{3,22}=U_3+U_J.$$

$$p_{2,23}=N_{2,\bar{\sigma}}b_{1,\bar{\sigma}}b_{3,\sigma};$$

$$\Pi_{1,23}=U_1+U_I,\Pi_{2,23}=U_2+U_I+U_J,\Pi_{3,23}=2U_J.$$

$$p_{2,24}=N_{2,\bar{\sigma}}b_{1,\bar{\sigma}}c_3;$$

$$\Pi_{1,24}=U_1+U_I,\Pi_{2,24}=U_2+U_I+2U_J,\Pi_{3,24}=U_3+2U_J.$$

$$p_{2,25}=N_{2,\bar{\sigma}}b_{1,\sigma}a_3;$$

$$\Pi_{1,25}=2U_I,\Pi_{2,25}=U_2+U_I,\Pi_{3,25}=U_J.$$

$$p_{2,26}=N_{2,\bar{\sigma}}b_{1,\sigma}b_{3,\bar{\sigma}};$$

$$\Pi_{1,26}=2U_I,\Pi_{2,26}=U_2+U_I+U_J,\Pi_{3,26}=U_3+U_J.$$

$$p_{2,27}=N_{2,\bar{\sigma}}b_{1,\sigma}b_{3,\sigma};$$

$$\Pi_{1,27}=2U_I,\Pi_{2,27}=U_2+U_I+U_J,\Pi_{3,27}=2U_J.$$

$$p_{2,28}=N_{2,\bar{\sigma}}b_{1,\sigma}c_3;$$

$$\Pi_{1,28}=2U_I,\Pi_{2,28}=U_2+U_I+2U_J,\Pi_{3,28}=U_3+2U_J.$$

$$p_{2,29}=N_{2,\bar{\sigma}}c_1a_3;$$

$$\Pi_{1,29}=U_1+2U_I,\Pi_{2,29}=U_2+2U_I,\Pi_{3,29}=U_J.$$

$$p_{2,30}=N_{2,\bar{\sigma}}c_1b_{3,\bar{\sigma}};$$

$$\Pi_{1,30}=U_1+2U_I,\Pi_{2,30}=U_2+2U_I+U_J,\Pi_{3,30}=U_3+U_J.$$

$$p_{2,31}=N_{2,\bar{\sigma}}c_1b_{3,\sigma};$$

$$\Pi_{1,31}=U_1+2U_I,\Pi_{2,31}=U_2+2U_I+U_J,\Pi_{3,31}=2U_J.$$

$$p_{2,32}=N_{2,\bar{\sigma}}c_1c_3;$$

$$\Pi_{1,32}=U_1+2U_I,\Pi_{2,32}=U_2+2U_I+2U_J,\Pi_{3,32}=U_3+2U_J.$$

$G^r_{3,m}(\epsilon)$ is obtained from $G^r_{1,m}(\epsilon)$ by exchanging the indices 1 and 3. The average occupation numbers $N_{\ell,\sigma}$, $N_{\ell,\bar{\sigma}}$, and c_ℓ are determined by solving Eqs. (18) and (19).

---

[1] A. J. Minnich, M. S. Dresselhaus, Z. F. Ren, and G. Chen, Energy Environ Sci **2** 466 (2009).

[2] M. Zebarjadi, K. Esfarjania, M.S. Dresselhaus, Z.F. Ren and G. Chen, Energy Environ Sci **5** 5147 (2012).

[3] G. Mahan, B. Sales and J. Sharp, Physics Today **50** (3) 42 (1997).

[4] R. Venkatasubramanian, E. Siivola, T. Colpitts, B. O'Quinn, Nature **413** 597 (2001).

[5] A. I. Boukai, Y. Bunimovich, J. Tahir-Kheli, J. K. Yu, W. A. Goddard III, and J. R. Heath, Nature **451** 168 (2008).

[6] T. C. Harman, P. J. Taylor, M. P. Walsh, and B. E. LaForge, Science **297** 2229 (2002).

[7] K. F. Hsu, S. Loo, F. Guo,W. Chen, J. S. Dyck, C. Uher, T. Hogan, E. K. Polychroniadis, and M. G. Kanatzidis, Science **303** 818 (2004).

[8] M. S. Dresselhaus, G. Chen, M. Y. Tang, R. Yang, H. Lee, D. Wang, Z. Ren, J. P. Fleurial, and P. Gogna, Adv. Mater. **19**, 1043 (2007).

[9] Y. M. Lin, and M. S. Dresselhaus, Phys. Rev. B **68**, 0 75304 (2003).

[10] P. Murphy, S. Mukerjee, and J. Moore, Phys. Rev. B **78**, 161406 (2008).

[11] D. M. T. Kuo, and Y. C. Chang, Phys. Rev. B **81** 0205321 (2010).

[12] D. M. T. Kuo, S. Y. Shiau, and Y. C. Chang, Phys. Rev. B, **84**, 245303 (2011).

[13] D. M. T. Kuo, and Y. C. Chang, Nanoscale research letters. **7**, 257 (2012).

[14] P. W. Anderson, P. A. Lee, M. Randeria, T. M. Rice, N. Trivedi, and F. C. Zhang, J. Phys. Condens, Matter **16**, R755 (2004).

[15] Y. Meir and N. S. Wingreen, Phys. Rev. Lett. **68,** 2512

(1992).

[16] Y. Liu, Y. S. Zheng, W. J. Gong, and T. Q. Lu, Phys. Lett. A **360**, 154 (2006).

[17] T. Markussen, A. P. Jauho, and M. Brandbyge, Phys. Rev. Lett. **103**, 055502 (2009).

[18] D. H. Santamore and M. C. Cross, Phys. Rev. Lett. **87**, 115502 (2001).

[19] L. G. C. Rego and G. Kirczenow, Phys. Rev. Lett. **81**, 232 (1998).

[20] K. Schwab, E. A. Henriksen, J. M. Worlock, and M. L. Roukes, Nature **404**, 974 (2000).

[21] A. Khitun, A. Balandin, J. L. Liu, and K. L. Wang, J. Appl. Phys. **88**, 696 (2000).

[22] D. L. Nika, E. P. Pokatilov, A. A. Balandin, V. M. Formin, A. Rastelli, and O. G. Schmidt, Phys. Rev. B **84**, 165415 (2011).

[23] F. R. Waugh, M. J. Berry, D. J. Mar, R. M. Westervelt, K. L. Campman, and A. C. Gossard, Phys. Rev. Lett. **75**, 705 (1995).

[24] S. Amaha, T. Hatano, H. Tamura, S. Teraoka, T. Kubo, Y. Tokura, D. G. Austing, and S. Tarucha, Phys. Rev. B **85**, 081301 (2012).

[25] I. Weymann, J. Phys. Condens. Matter **22**, 015301 (2010).

[26] C. Y. Hsieh, Y. Shim, and P. Hawrylak, Phys. Rev. B **85**, 085309 (2012).

[27] Z. T. Jiang, Q. F. Sun, and Y. Wang, Phys. Rev. B **72**, 045332 (2005).

[28] L. Oroszlany, A. Kormanyos, J. Koltai, J. Cserti, and C. J. Lambert, Phys. Rev. B **76**, 045318 (2007).

[29] J. Liu, Q. F. Sun, and X. C. Xie, Phys. Rev. B. **81**, 245323 (2010).

[30] M. Wierzbicki, and R. Swirkowicz, Phys. Rev. B **84**, 075410 (2011).

[31] F. Chi, J. Zheng, X. D. Lu, and K. C. Zhang, Phys. Lett. A, **375**, 1352 (2011).

[32] P. Trocha, and J. Barnas, Phys. Rev. B **85**, 085408 (2012).

[33] S. Doniach, and E. H. Sondheimer, "Green's functions for Solid State Physics", Imperial College Press 1998.

[34] G. Beni, Phys. Rev. B **10,** 2186 (1974).

[35] R. A. Bari, Phys. Rev. B **10**, 1560 (1974).

[36] J. F. Kwak, and G. Beni, Phys. Rev. B **13**, 652 (1976).

[37] P. Mani, N. Nakpathomkun, E. A. Hoffmann, and H. Linke, Nano Letters, **11**, 4679 (2011).

Figure Captions

Fig. 1. (a) Schematics for a chain of coupled quantum dots (CCQD) connected to metallic electrodes, where T_L and T_R describe the equilibrium temperature of the left and right electrodes, respectively. (b) The band diagram illustrating a CCQD connected to metallic electrodes.

Fig. 2. Electrical conductance (G_e), Seebeck coefficient (S) and electrical thermal conductance (κ_e) as functions of gate voltage (V_g), which is used to tune the E_3 level for various temperatures. $E_1 = E_2 = E_F - 20\Gamma_0$, $E_3 = E_F + 30\Gamma_0 - eV_g$. $U_\ell = 60\Gamma_0$, $U_{\ell,j} = 20\Gamma_0$, $t_{\ell,j} = 1\Gamma_0$, and $\Gamma_L = \Gamma_R = \Gamma_0$.

Fig. 3. Electrical conductance (G_e), Seebeck coefficient (S) and electrical thermal conductance (κ_e) as functions of gate voltage (V_g), which is used to tune the E_2 level for various temperatures. $E_1 = E_F - 20\Gamma_0$, $E_2 = E_F + 10\Gamma_0 - eV_g$, and $E_3 = E_F$. Other physical parameters are the same as those of Fig. 2.

Fig. 4. Occupation number (N), electrical conductance (G_e), and Seebeck coefficient (S) as functions of gate voltage (V_g), which is used to tune the E_2 level for various temperatures. $E_1 = E_F - 10\Gamma_0$, $E_2 = E_F + 10\Gamma_0 - eV_g$, and $E_3 = E_F - 60\Gamma_0$. $U_{\ell,j} = 10\Gamma_0$. Other physical parameters are the same as those of Fig. 2.

Fig. 5. Occupation number (N), electrical conductance (G_e), Seebeck coefficient (S), and electrical thermal conductance (κ_e) as functions of gate voltage (V_g) at low temperature ($k_BT = 1\Gamma_0$) for QDs with identical energy levels $E_\ell = E_F + 30\Gamma_0 - eV_g$. Other physical parameters are the same as those of Fig. 2.

Fig. 6. Electrical conductance (G_e), Seebeck coefficient (S), and ZT as functions of detuning energy, $\Delta = E_\ell - E_F$ at temperature $k_BT = 10\Gamma_0$ with and without interdot Coulomb interactions.

Fig. 7. Electrical conductance G_e, Seebeck coefficient (S), and ZT as functions of gate voltage (V_g) at temperature $k_BT = 10\Gamma_0$ for various interdot Coulomb interactions. $E_\ell = E_F + 30\Gamma_0 - eV_g$ and $\Gamma_L = \Gamma_R = \Gamma_0$.

Fig. 8. G_e, S, κ_e, and ZT as functions of temperature for CCQDs with the QD number N varying from 2 to 5. Symmetrical tunneling rates $\Gamma_L = \Gamma_R = \Gamma_0$ $are used. E_\ell = E_0 = E_F + 30\Gamma_0$, intradot Coulomb interactions $U_\ell = U = 30\Gamma_0$, and electron hopping strengths $t_{\ell,j} = t_c = 3\Gamma_0.\Gamma_L = \Gamma_R = \Gamma = \Gamma_0$

Fig. 9. Electron occupation number (N), electrical conductance (G_e), Seebeck coefficient (S), and ZT as functions of gate voltage (V_g) for various temperatures. $U = 30\Gamma_0$, $t_c = 3\Gamma_0$, and $\Gamma = \Gamma_0$.

Fig. 10. G_e, S, (ZT)$_0$, and ZT as functions of t_c at $k_BT = 10\Gamma_0$ for various detuning energies. $U = 60\Gamma_0$ and $\Gamma = \Gamma_0$. The curves marked by filled triangles and diamonds in Fig. 4(d) are for $\Delta = 30\Gamma_0$), but with asymmetric tunneling rates $\Gamma_L \neq \Gamma_R$.

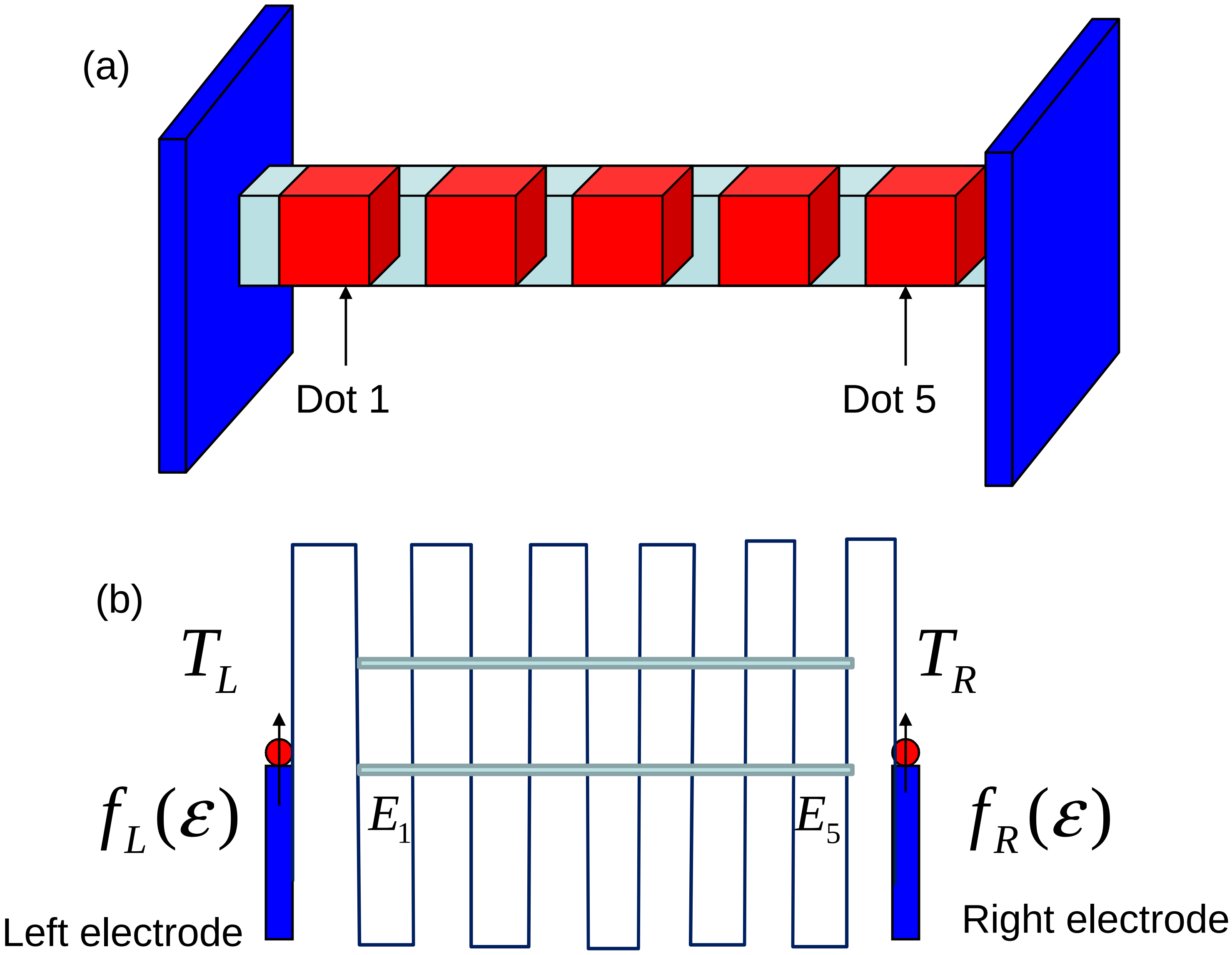
(a)
Dot 1
Dot 5
(b)
T_L
T_R
$f_L(\varepsilon)$
E_1
E_5
$f_R(\varepsilon)$
Left electrode
Right electrode

Fig1

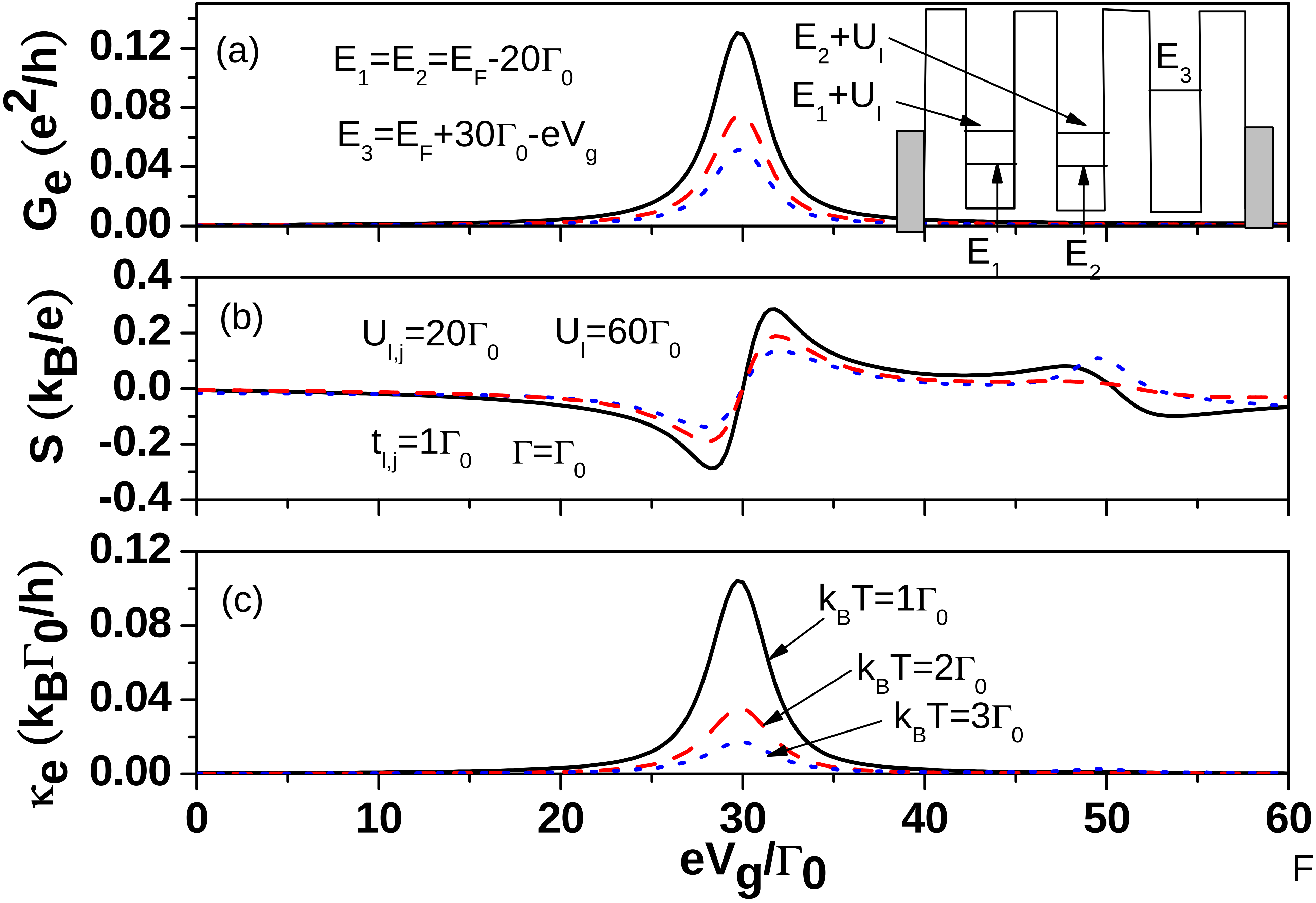
(a)
$E_1=E_2=E_F-20\Gamma_0$
$E_3=E_F+30\Gamma_0-eV_g$
E_2+U_l
E_1+U_l
E_3
E_1
E_2
$G_e\ (e^2/h)$
0.12
0.08
0.04
0.00
(b)
$U_{l,j}=20\Gamma_0$
$U_l=60\Gamma_0$
$t_{l,j}=1\Gamma_0$
$\Gamma=\Gamma_0$
$S\ (k_B/e)$
0.4
0.2
0.0
-0.2
-0.4
(c)
$k_BT=1\Gamma_0$
$k_BT=2\Gamma_0$
$k_BT=3\Gamma_0$
$\kappa_e\ (k_B\Gamma_0/h)$
0.12
0.08
0.04
0.00
0
10
20
30
40
50
60
eV_g/Γ_0

Fig2

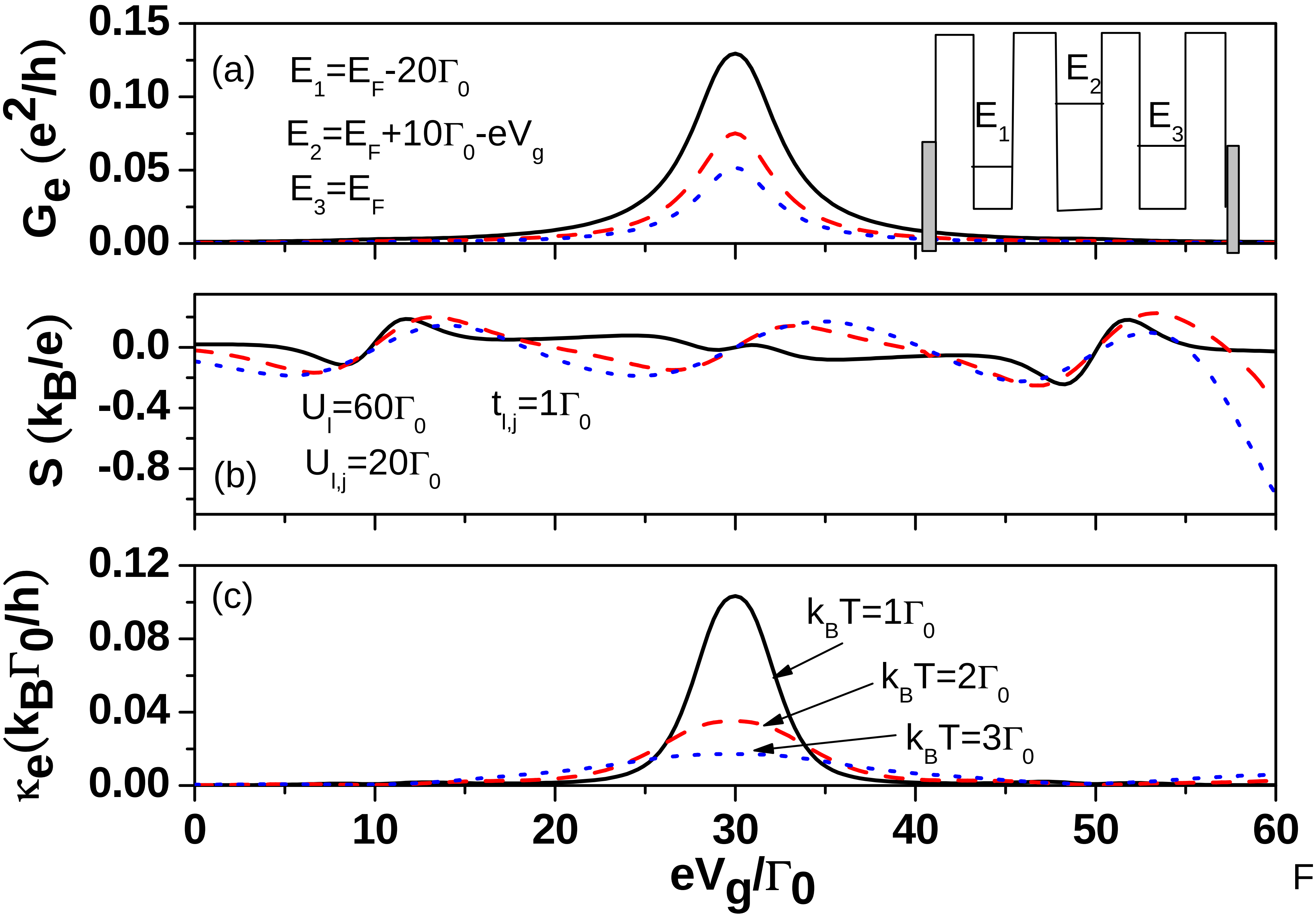
(a)
$E_1=E_F-20\Gamma_0$
$E_2=E_F+10\Gamma_0-eV_g$
$E_3=E_F$
E_1
E_2
E_3
$G_e\ (e^2/h)$
0.15
0.10
0.05
0.00
(b)
$U_l=60\Gamma_0$
$t_{l,j}=1\Gamma_0$
$U_{l,j}=20\Gamma_0$
$S\ (k_B/e)$
0.0
-0.4
-0.8
(c)
$k_BT=1\Gamma_0$
$k_BT=2\Gamma_0$
$k_BT=3\Gamma_0$
$\kappa_e(k_B\Gamma_0/h)$
0.12
0.08
0.04
0.00
0
10
20
30
40
50
60
eV_g/Γ_0

Fig3

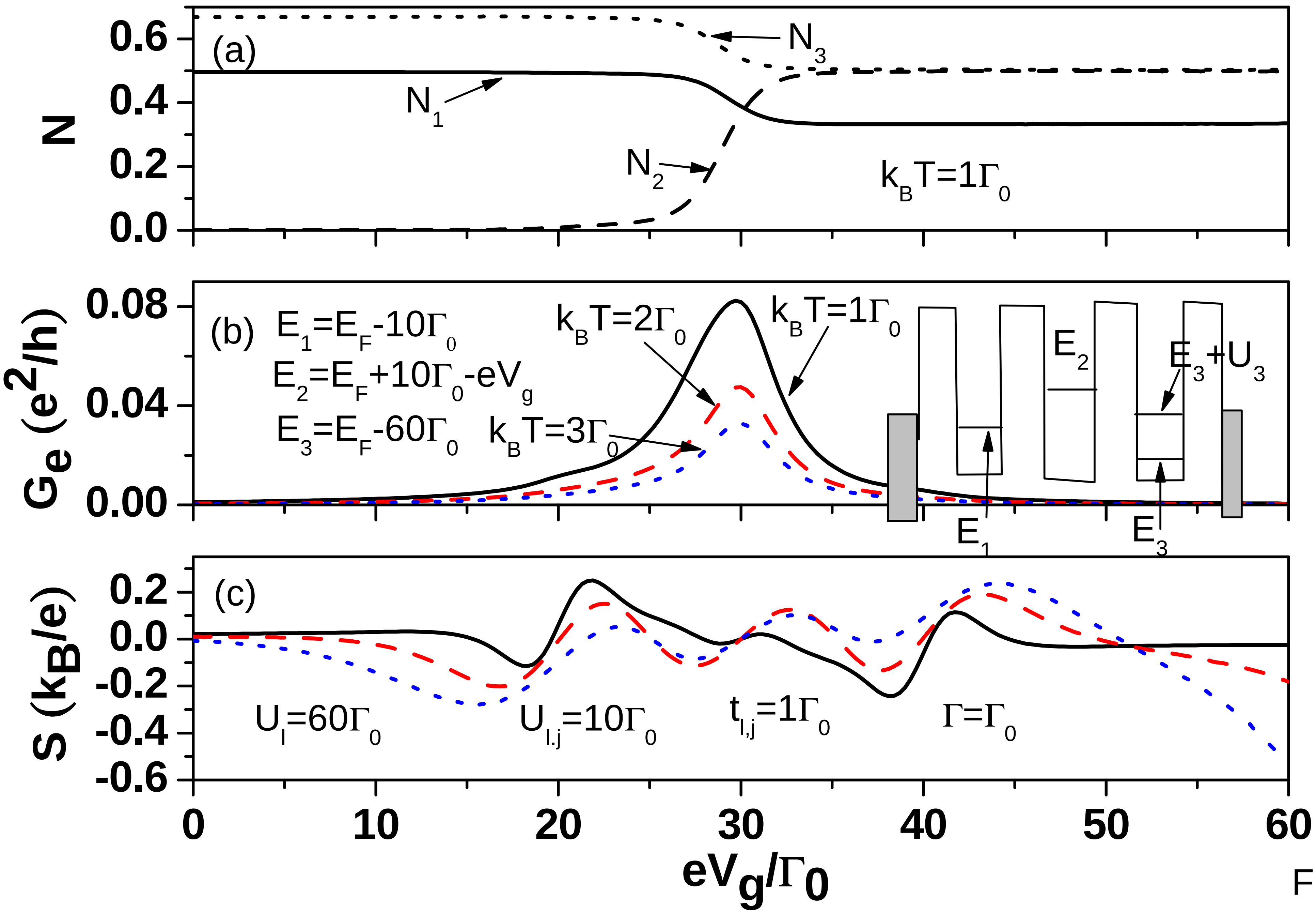
N
0.6
0.4
0.2
0.0
(a)
N_3
N_1
N_2
k_BT=1Γ_0
G_e (e^2/h)
0.08
0.04
0.00
(b)
E_1=E_F-10Γ_0
E_2=E_F+10Γ_0-eV_g
E_3=E_F-60Γ_0
k_BT=2Γ_0
k_BT=1Γ_0
k_BT=3Γ_0
E_2
E_3+U_3
E_1
E_3
S (k_B/e)
0.2
0.0
-0.2
-0.4
-0.6
(c)
U_l=60Γ_0
U_l,j=10Γ_0
t_l,j=1Γ_0
Γ=Γ_0
0
10
20
30
40
50
60
eV_g/Γ_0

Fig4

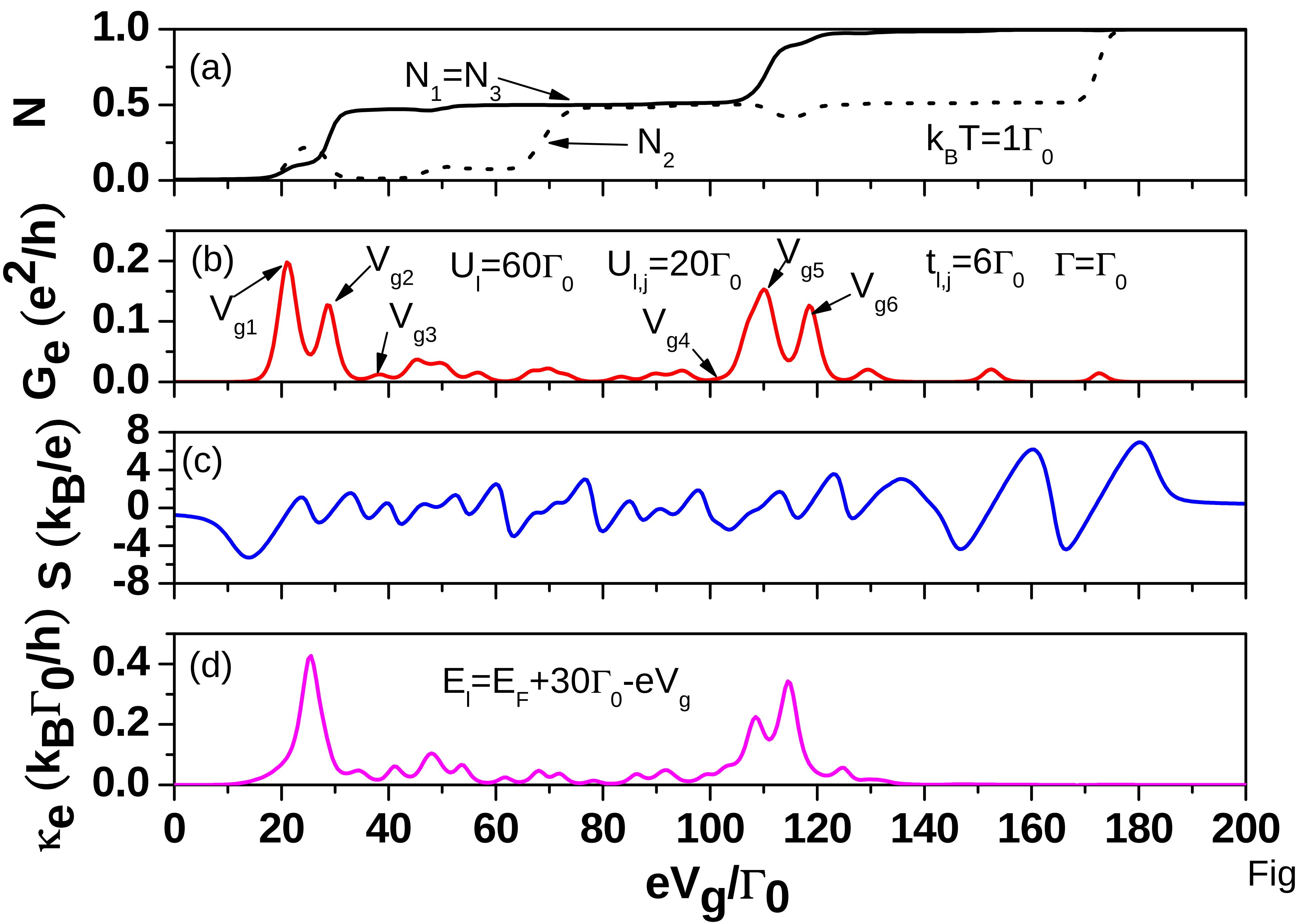
(a)
(b)
(c)
(d)
N
$N_1=N_3$
N_2
$k_BT=1\Gamma_0$
1.0
0.5
0.0
G_e (e^2/h)
0.2
0.1
0.0
V_{g1}
V_{g2}
V_{g3}
V_{g4}
V_{g5}
V_{g6}
$U_l=60\Gamma_0$
$U_{l,j}=20\Gamma_0$
$t_{l,j}=6\Gamma_0$
$\Gamma=\Gamma_0$
S (k_B/e)
8
4
0
-4
-8
κ_e ($k_B\Gamma_0/h$)
0.4
0.2
0.0
$E_l=E_F+30\Gamma_0-eV_g$
0
20
40
60
80
100
120
140
160
180
200
eV_g/Γ_0

Fig5

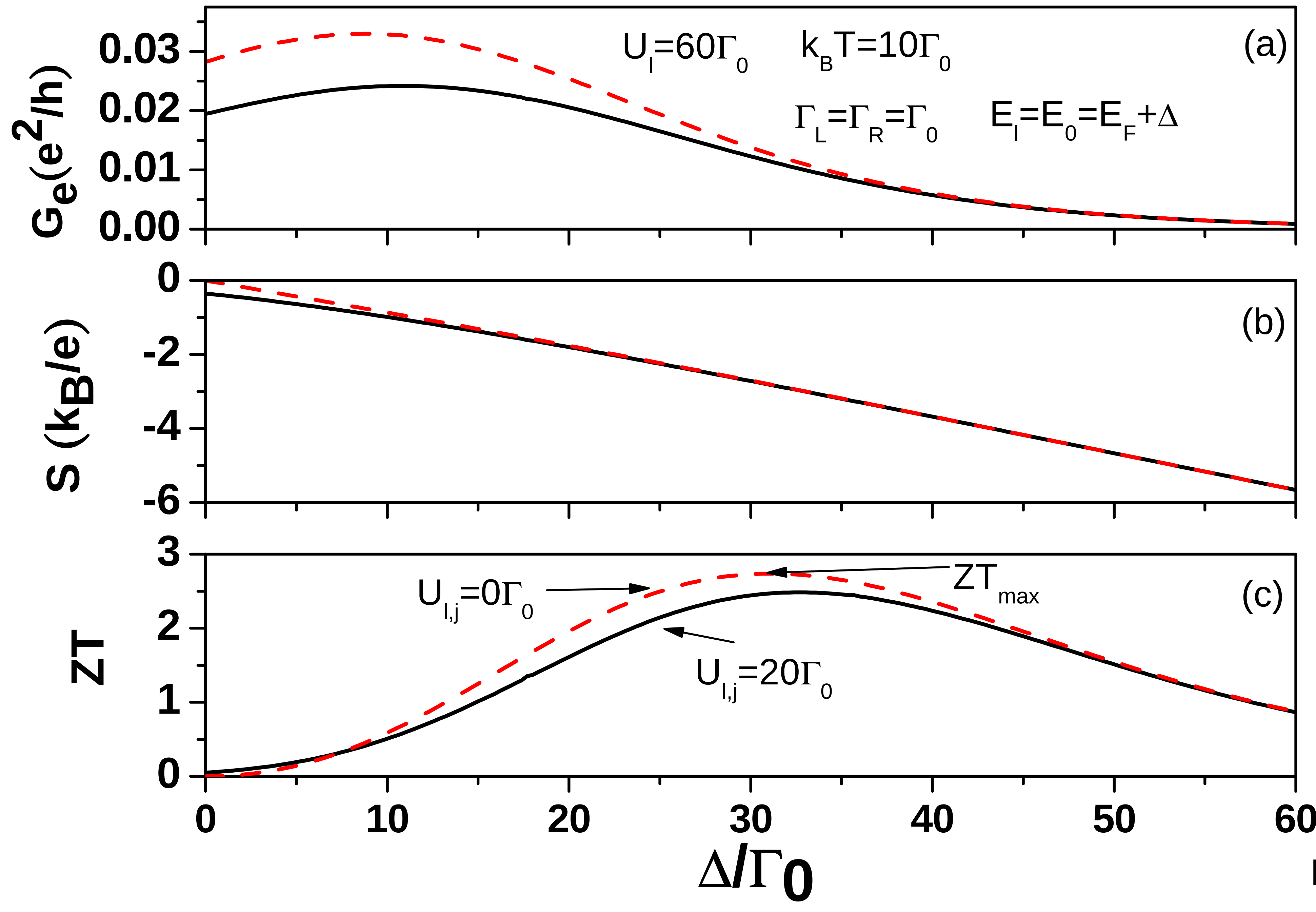

G_e(e^2/h)
0.03
0.02
0.01
0.00
U_l=60Γ_0
k_BT=10Γ_0
Γ_L=Γ_R=Γ_0
E_l=E_0=E_F+Δ
(a)
S (k_B/e)
0
-2
-4
-6
(b)
ZT
3
2
1
0
U_l,j=0Γ_0
ZT_max
U_l,j=20Γ_0
(c)
0
10
20
30
40
50
60
Δ/Γ0

Fig6

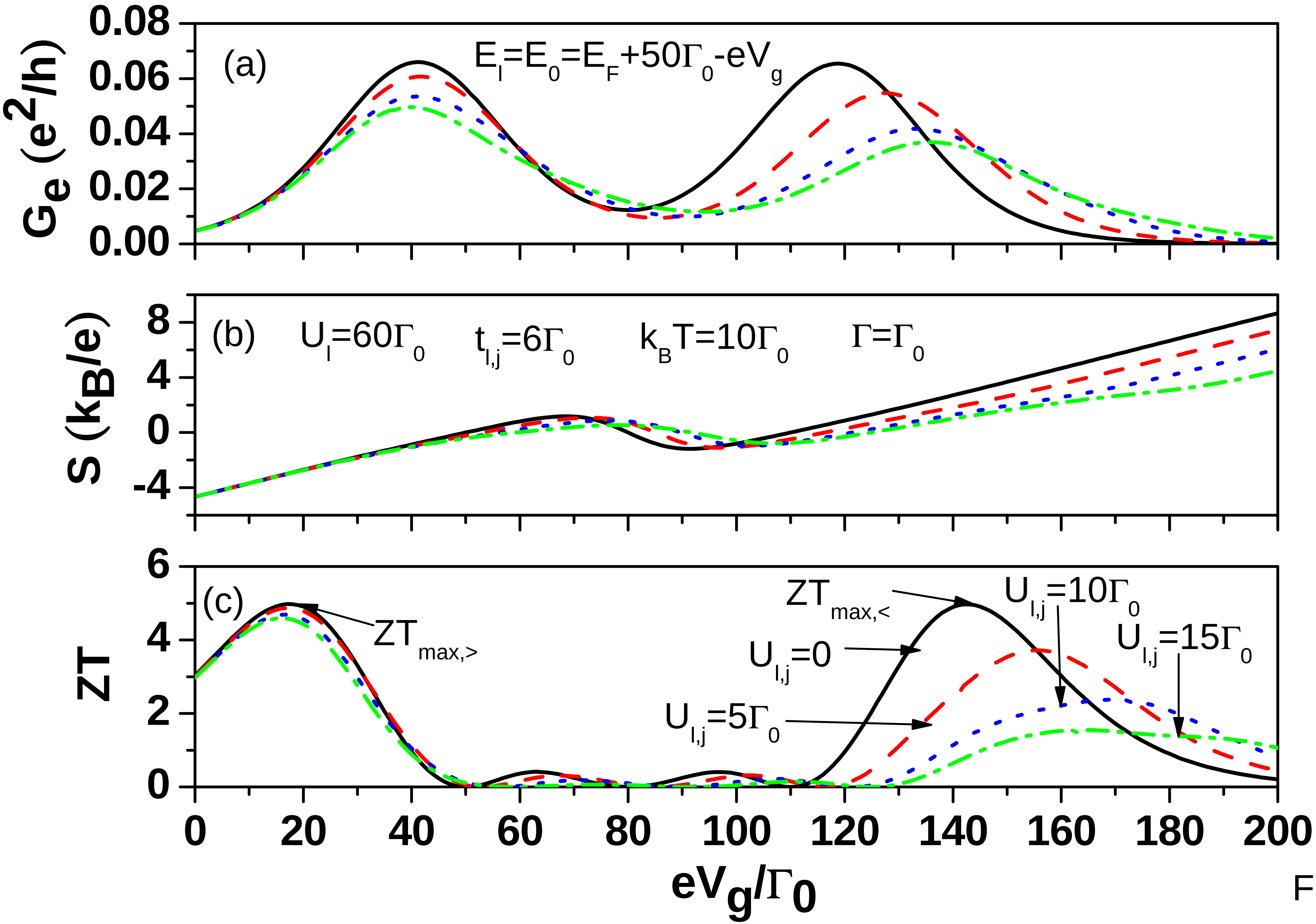
(a)
$E_l=E_0=E_F+50\Gamma_0-eV_g$
G_e (e^2/h)
0.00
0.02
0.04
0.06
0.08
(b)
$U_l=60\Gamma_0$
$t_{l,j}=6\Gamma_0$
$k_BT=10\Gamma_0$
$\Gamma=\Gamma_0$
S (k_B/e)
-4
0
4
8
(c)
ZT
0
2
4
6
$ZT_{max,>}$
$ZT_{max,<}$
$U_{l,j}=0$
$U_{l,j}=5\Gamma_0$
$U_{l,j}=10\Gamma_0$
$U_{l,j}=15\Gamma_0$
0
20
40
60
80
100
120
140
160
180
200
eV_g/Γ_0

Fig7

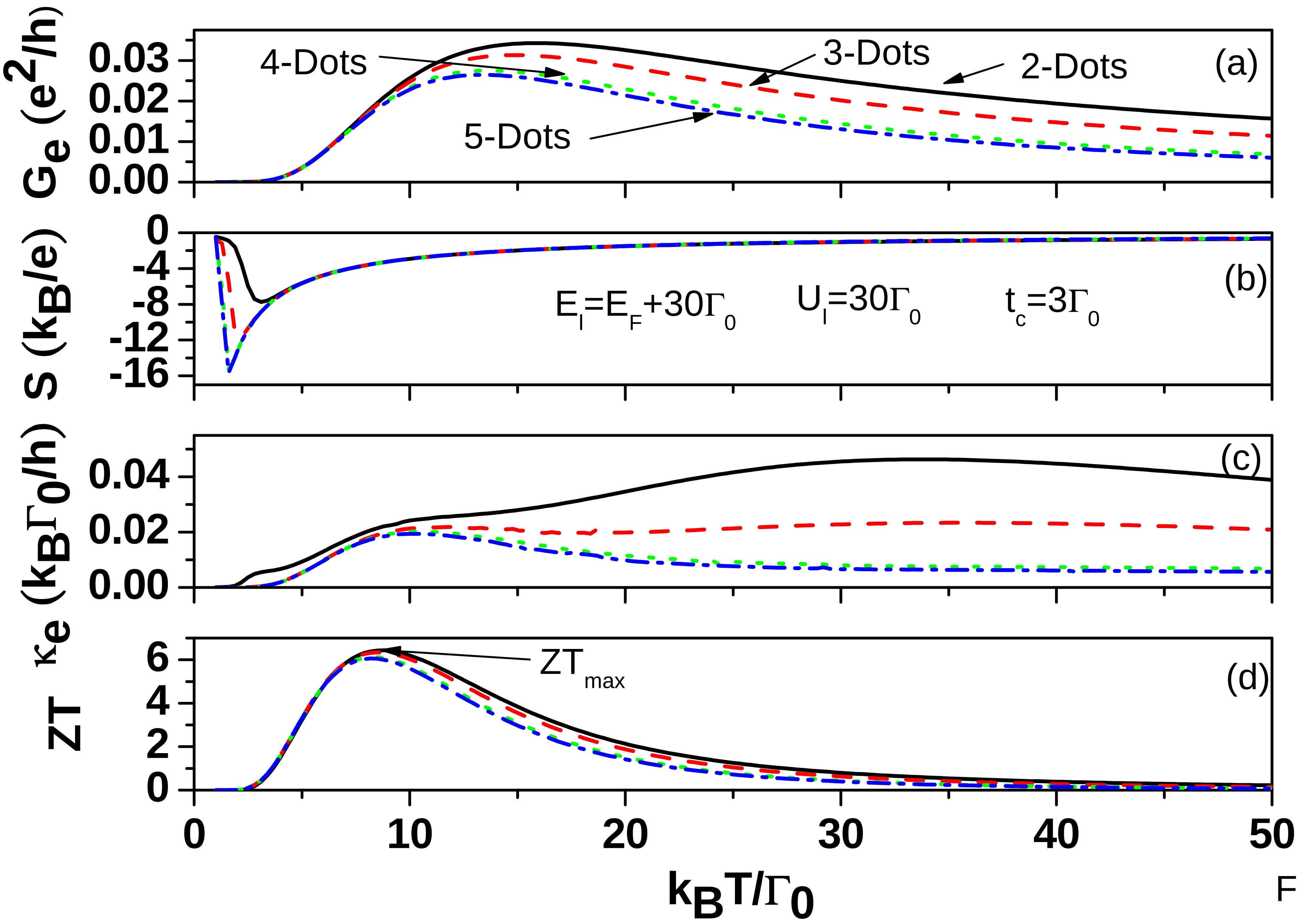

G_e (e^2/h)
0.03
0.02
0.01
0.00
4-Dots
3-Dots
2-Dots
5-Dots
(a)
S (k_B/e)
0
-4
-8
-12
-16
(b)
$E_l=E_F+30\Gamma_0$
$U_l=30\Gamma_0$
$t_c=3\Gamma_0$
κ_e $(k_B\Gamma_0/h)$
0.04
0.02
0.00
(c)
ZT
6
4
2
0
ZT_{max}
(d)
0
10
20
30
40
50
k_BT/Γ_0

Fig8

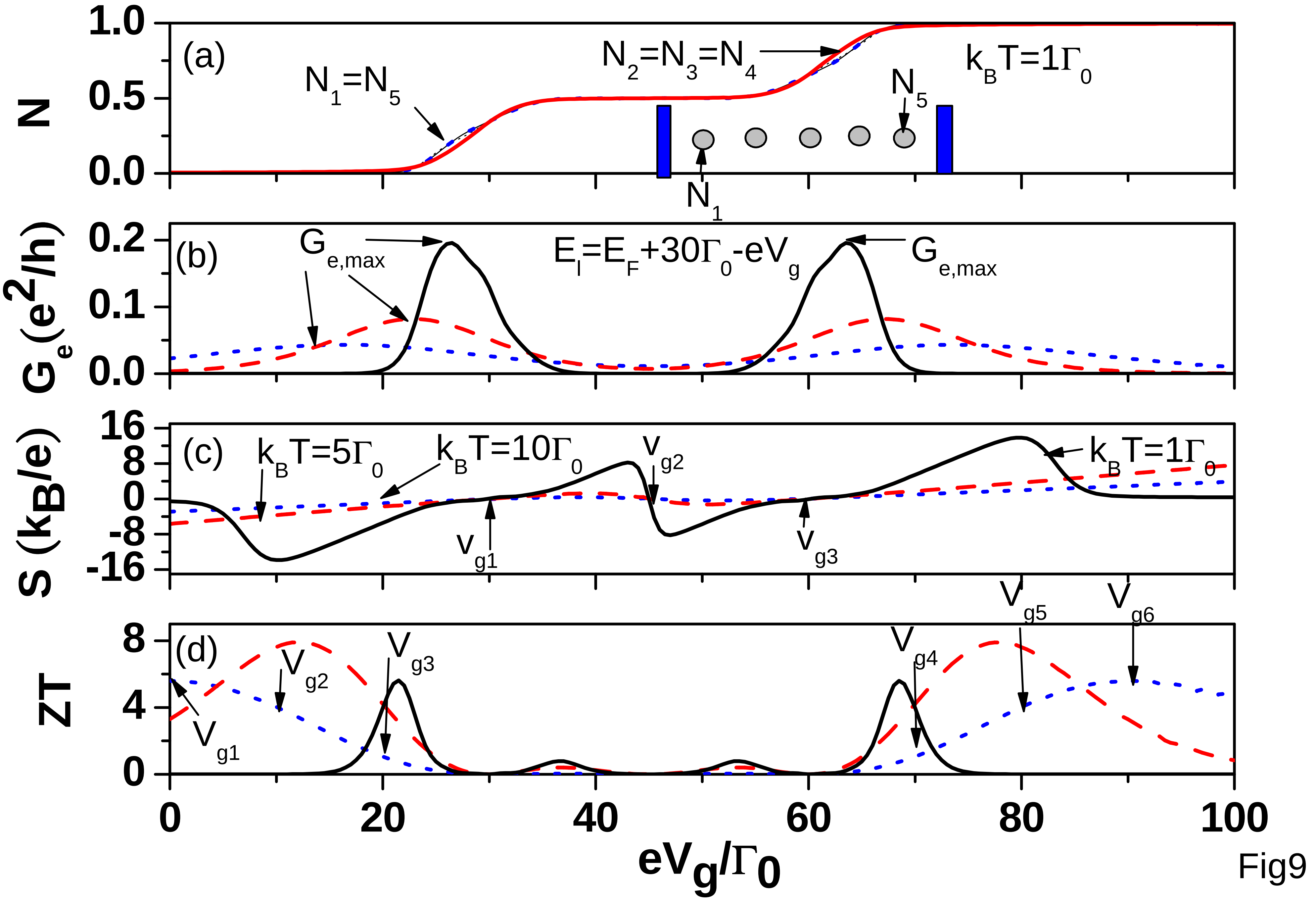
N
1.0
0.5
0.0
(a)
N1=N5
N2=N3=N4
kBT=1Γ0
N5
N1
Ge(e2/h)
0.2
0.1
0.0
(b)
Ge,max
El=EF+30Γ0-eVg
Ge,max
S (kB/e)
16
8
0
-8
-16
(c)
kBT=5Γ0
kBT=10Γ0
Vg2
kBT=1Γ0
Vg1
Vg3
Vg5
Vg6
ZT
8
4
0
(d)
Vg2
Vg3
Vg4
Vg1
0
20
40
60
80
100
eVg/Γ0

Fig9

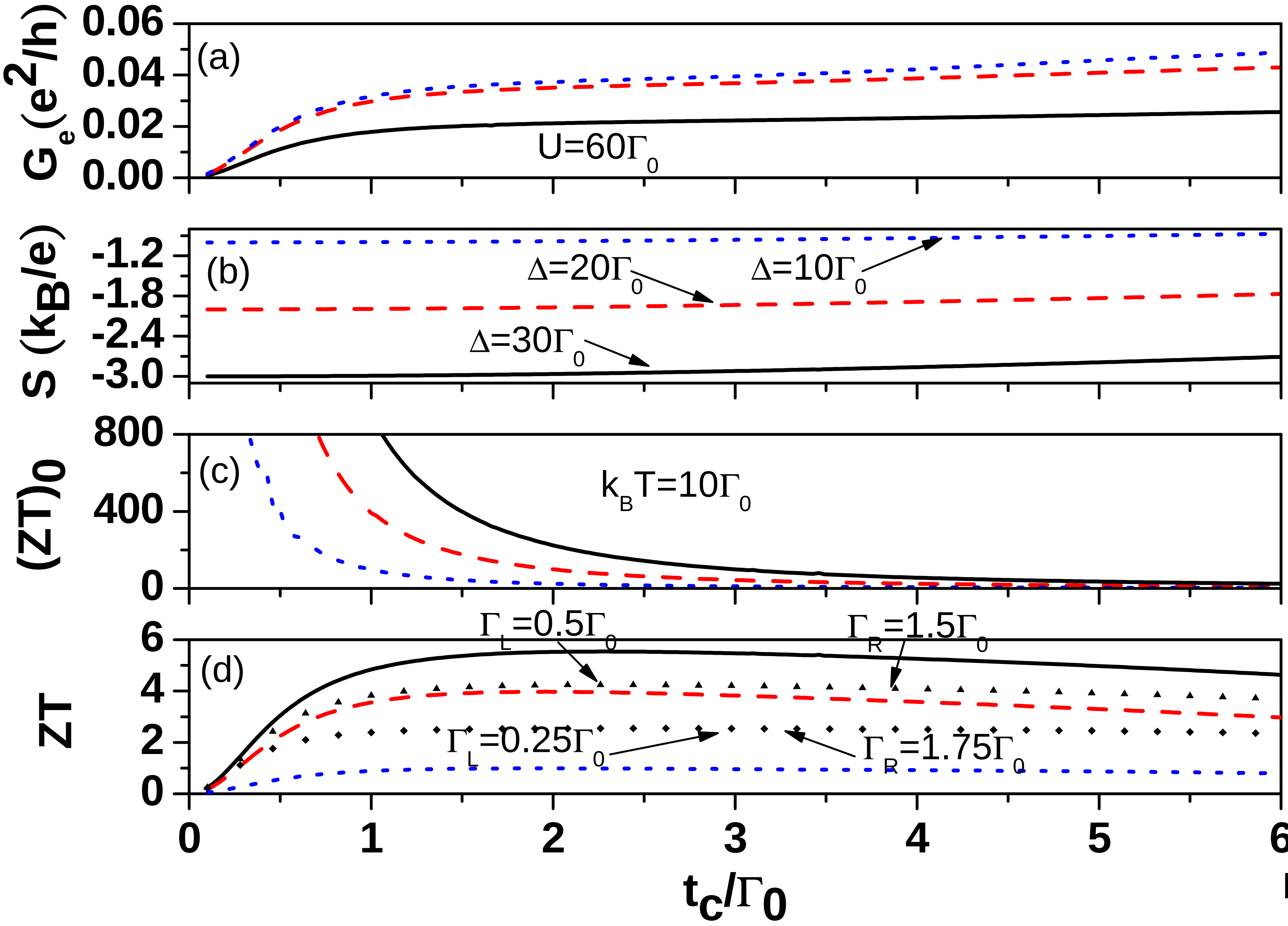
$G_e (e^2/h)$
0.06
0.04
0.02
0.00
(a)
$U=60\Gamma_0$
$S (k_B/e)$
-1.2
-1.8
-2.4
-3.0
(b)
$\Delta=20\Gamma_0$
$\Delta=10\Gamma_0$
$\Delta=30\Gamma_0$
$(ZT)_0$
800
400
0
(c)
$k_BT=10\Gamma_0$
ZT
6
4
2
0
(d)
$\Gamma_L=0.5\Gamma_0$
$\Gamma_R=1.5\Gamma_0$
$\Gamma_L=0.25\Gamma_0$
$\Gamma_R=1.75\Gamma_0$
0
1
2
3
4
5
6
t_c/Γ_0

Fig10